Chem Soc Rev

This article was published as part of the

From microfluidic application to nanofluidic phenomena issue

Reviewing the latest advances in microfluidic and nanofluidic research

Guest Editors Professors Albert van den Berg, Harold Craighead and Peidong Yang

Please take a look at the issue 3 table of contents to access other reviews in this themed issue

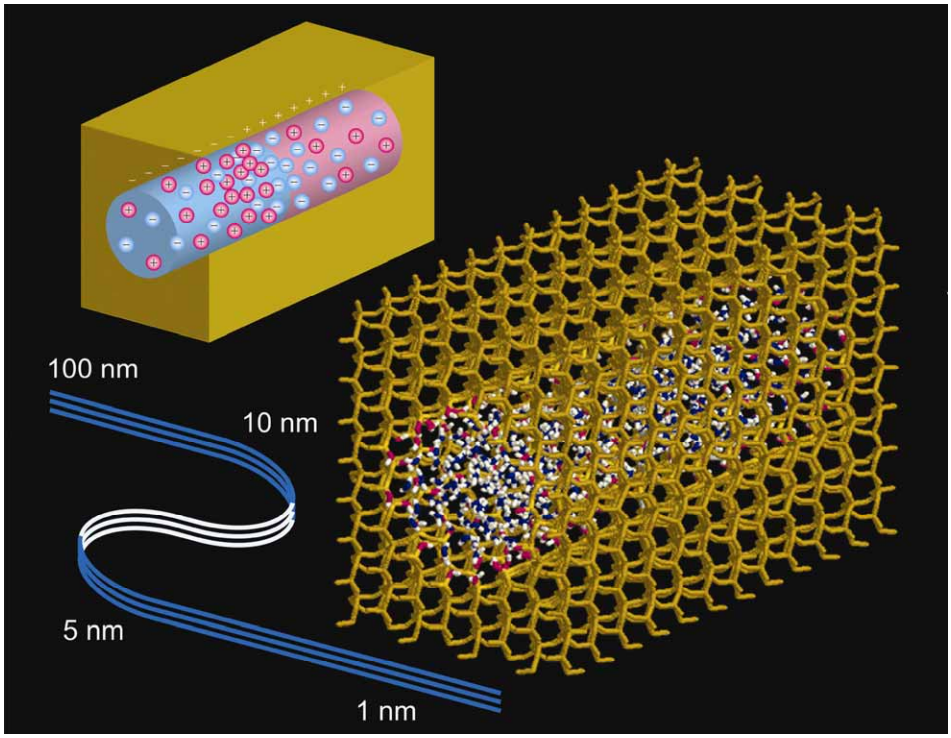

DNA manipulation, sorting, and mapping in nanofluidic systems†

Stephen L. Levy and Harold G. Craighead*

Received 17th August 2009
First published as an Advance Article on the web 12th January 2010
DOI: 10.1039/b820266b

Fluidic systems with nanometre length scales enable sensitive analysis of DNA molecules. Nanofluidic systems have been used to probe conformational, dynamic, and entropic properties of DNA molecules, to rapidly sort DNA molecules based on length dependent interactions with their confining environment, and for determining the spatial location of genetic information along long DNA molecules. In this *critical review*, recent experiments utilizing fluidic systems comprised of nanochannels, nanoslits, nanopores, and zero-mode waveguides for DNA analysis are reviewed (161 references).

A. Introduction

The quantitative study of individual DNA molecules confined within nanofluidic systems has become possible over the past decade due to advances in nanofabrication technology. The motivation for studying DNA molecules is provided by their fundamental biological role as carriers of the digital code that determines the development of cells in all living organisms. The recent promise of personalized medicine based on an individual's knowledge of particular gene sequences or mutations has spurred a tremendous interest in sensitive technologies capable of delivering inexpensive and high throughput sequencing platforms. Nanofluidic platforms are being actively utilized toward this end[1] as well as for quantitative gene expression and RNA analysis.[2] In addition to application driven interests, there are many fundamental biological questions that may best be approached by studying the dynamics of biomolecules in experimentally tunable nanostructures. These questions include the expression of genes based on chromatin conformation,[3] mechanisms responsible for bacterial chromosome separation during cell division,[4] packaging of long DNA strands in viral phages,[5] interactions with proteins responsible for transcribing DNA that search for specific binding sequences,[6] and the role of methylation in gene expression.[7]

The most frequently encountered reasons for using nanosystems for biomolecule analysis are the reduction in often expensive reagent, the ability for high throughput *via* large scale parallelization, and increased sensitivity of detection.[8] More fundamentally, biology takes place in a highly confined

School of Applied and Engineering Physics, Cornell University, Ithaca, NY 14853, USA. E-mail: hgc1@cornell.edu; Fax: +1 6072557658; Tel: +1 6072556286

† Part of the themed issue: From microfluidic application to nanofluidic phenomena.

Stephen L. Levy

Stephen Levy has been a Research Associate in the Applied and Engineering Physics Department of Cornell University since 2006. He received his Bachelor of Science degree in Physics and Math from the University of Richmond in 1997. He received his PhD in Physics from UC Santa Barbara in 2003 and then spent three years as a post-doctoral researcher at the University of Chicago. His research involves optical and electrical investigations of individual nucleic acid molecules within nanofluidic systems.

Harold G. Craighead

Harold Craighead received his Bachelor of Science Degree in Physics, from the University of Maryland in 1974. He received his PhD in Physics from Cornell University in 1980 after which he became a Member of Technical Staff at Bell Laboratories and Research Manager at Bellcore. Dr Craighead joined the faculty of Cornell University in 1989 as a Professor in the School of Applied and Engineering Physics and Director of the National Nanofabrication Facility. He has served as the Director of the School of Applied & Engineering Physics and as Interim Dean of the College of Engineering. Dr Craighead is currently the Director of the Nanobiotechnology Center. He is a member of the National Academy of Engineering, and he holds the Charles Lake Jr chaired professorship in Engineering at Cornell. His research focuses on investigating nanoscale devices and developing new approaches for creating and observing nanosystems.

environment: the ability to systematically study those processes that involve DNA as a function of confinement may yield important physical insights to the biological processes previously listed. The ability to study single DNA molecules may reveal distinct subpopulations hidden underneath the mean behavior from measurements that average over DNA from thousands of cells. Further, novel approaches to investigating DNA are opened since the governing physics of the nanoscale is qualitatively different than that of the macro world (high resolution near field microscopy, for example).

We begin this review with a brief overview of some nomenclature and a general description of the type of experiments that are discussed herein. When referring to a nanofluidic system, we typically mean a fabricated fluid filled structure whose defining boundaries are on the length scale of tens or hundreds of nanometres. For a structure one hundred nanometres wide and deep, with a length of one micron, this implies a contained volume of 10 attolitres (approximately one millionth the volume of a eukaryotic cell). There are essentially three basic types of structures that are used for DNA investigation, referred to here as nanochannels, nanoslits, and nanopores. A nanoslit contains one nanoscale dimension (depth), restricting DNA to movement within a plane. A nanochannel contains two nanoscale dimensions (width and depth) and one microscale dimension (length), restricting DNA to movement along a line. A nanopore contains three nanoscale dimensions with axial symmetry (radius and length). Nanofluidic systems contain larger structures that interface to the nanofeature on one side and eventually to the macro world on the other. In all cases, it is the nanostructure (or interface to this structure) that allows for the sensitive investigation of individual DNA molecules. As the dividing line between a sub-microfluidic and nanofluidic system is rather arbitrary, we will also discuss microfluidic devices where pertinent results have been obtained. There are a variety of detection schemes for measuring a biological or physical aspect of DNA in a confined fluidic system, but the most prevalent reviewed here consists of fluorescence microscopy whereby the DNA is stained with a dye, illuminated by an optical source at the dye's excitation wavelength, and the resulting fluorescent emission is measured with a photodetector. When referring generically to a DNA molecule, we mean one that is double stranded and will explicitly write single stranded otherwise. In a typical experiment, a buffer containing a dilute DNA concentration (~picomolar) is introduced into a reservoir *via* a pipette. The DNA is electrophoretically driven to or through the nanostructure, illuminated, and detected using a high numerical aperture objective. A schematic illustration of a nanochannel device is displayed in Fig. 1.

The three broad types of experiments that will be reviewed in detail are referred to as manipulating, sorting, and mapping of DNA. In an experiment that manipulates DNA, individual molecules are positioned within or across a nanostructure in order to measure a physical parameter describing the interaction of the molecule with its confined environment. The larger questions investigated with such experiments concern how both the static and dynamic properties of the molecule are altered from their values in bulk solution when subjected to

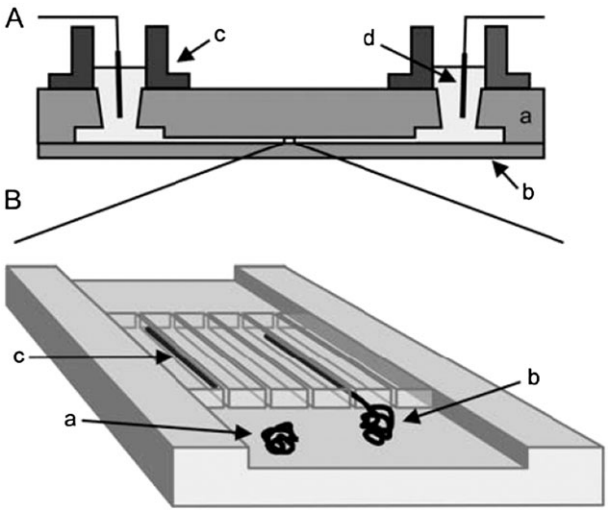

Fig. 1 Schematic representations of a nanofluidic structure for single molecule DNA analysis. (A) Side view schematic representation of an optically transparent substrate wafer (b) that is bonded to a cover slip wafer (a). DNA molecules are loaded into fluidic reservoirs (c) and driven electrophoretically using gold electrodes (d). (B) Schematic close-up view of the nanofluidic array region that contains a microfluidic loading region for DNA molecules (a), a DNA molecule partially inserted inside a nanochannel (b), and a linearized DNA molecule inside a nanochannel (c). Reprinted from ref. 9 with permission from © Biophysical Society (2006).

confining boundary conditions. For example, forcing a molecule to enter a structure smaller than its natural length in bulk solution changes the molecule's shape, which then alters the friction between the molecule and the solvent, and its diffusion coefficient. The complexity in predicting these confined properties is primarily introduced by the non-linear feedback between motions of non-neighboring segments of the molecule as mediated by the solvent and its assumed no-slip boundary condition at the walls of the nanostructure. Sorting experiments seek to exploit a length based mobility dependence to spatially or temporally separate different sized DNA molecules by transporting them through an array of nanostructures. Sorting of DNA fragments by size using polyacrylimide gels has been an essential tool of the widely used Sanger sequencing[10] method and sorting with nanofluidic chips (without gels) offers a compelling alternative for larger molecules. Finally, we review nanofluidic systems used for mapping genetic information along individual DNA molecules. Mapping consists of determining the location of a known short sequence at multiple locations along a DNA molecule (creating a so-called barcode of the DNA). In this category we also include DNA sequencing as the limit of mapping at all locations along a molecule.

In the following sections we will present a brief review of the relevant physics necessary to describe DNA within nanofluidic systems, followed by general fabrication strategies employed for constructing such devices, and then a critical review of interesting nanofluidic experiments involving manipulating, sorting, and mapping DNA in these devices. We note that several excellent reviews have already been written covering many topics that we will also discuss. We recommend reviews

concerning the following topics: one similar in scope to this review but outdated by recent results,[11] confined polymer behavior from experts in nanoslit experiments,[12] DNA linearization in nanofluidic channels,[13] transport phenomena in nanofluidic structures,[14] scaling laws for confined polymers,[15] fluorescent detection of biomolecules in nanostructures,[16] electrophoretic separation of DNA in nanostructures,[17] the relevant forces and phenomena in nanofluidic systems,[18] nanofilters for molecular sieving,[19] and DNA interactions with solid-state nanopores.[20]

B. Theory

To describe the physics underlying nanofluidic manipulations of DNA requires a mathematical description for confined DNA as well as for the chemical properties of an electrolytic buffer solution within a nanofluidic structure. We assume the reader is familiar with the molecular structure of double-stranded DNA[21] and briefly review its salient physical features. The common helical form of DNA within cells (B-DNA) has a contour length $L = Na$, where N is the number of base pairs, and a is the 0.34 nm distance between base pairs, and a physical width (w) of approximately 2 nm. The linear charge density due to the phosphate group is $-2q/a \approx -6q$/nm, where q is the charge of an electron. The molecule is referred to as a semi-flexible polymer, meaning qualitatively that it exhibits flexibility on long length scales and stiffness on short scales with the crossover set by a parameter termed the persistence length (p). The persistence length is more formally the characteristic distance over which the correlation between vectors tangent to the contour exponentially decays[22] and is approximately 50 nm (*in vivo* or typical $\sim$50 mM ionic concentration solutions used in experiments). This distance depends on the linear charge density and consequently on the ionic strength of the solution as will be discussed in Section D.2.

B.1 Unconfined polymers

The equilibrium size of an unconfined DNA molecule (typically given by the rms end-to-end length, R_0, or radius of gyration which is related by a numerical factor) is determined by a balance of opposing forces related to entropy and self-repulsion. Considering the former alone, simple random-walk statistics lead to the length scaling as $R_0 \approx (pL)^{1/2}$ and to a Gaussian probability distribution for the end-to-end vector $\boldsymbol{r}$:

$$p(\boldsymbol{r}) \approx \exp(-2\boldsymbol{r}^2/3R_0^2) \quad (1)$$

Since the entropy is the logarithm of this probability, we find that the polymer's free energy has an entropic spring-like term proportional to $\boldsymbol{r}^2$. The force required to extend a molecule to 30% of its contour length has been measured[23] to be 40 fN. The random-walk model, however, does not account for the inability of segments separated along the contour to occupy the same space. The self-avoidance, or excluded volume, of these segments due to electrostatic repulsion causes the chain to swell, resulting in $R_0 \approx (pw)^{1/5}L^{3/5}$.

B.2 Confined polymers

Confining a polymer within a nanostructure with a dimension d (either nanochannel diameter or nanoslit depth) smaller than the unconfined length R_0 causes the polymer to deform. The concept of blob theory was developed by de Gennes and colleagues[15,24–27] to describe the resulting conformation and dynamics of polymers confined to geometries with $R_0 > d > p$. The basic idea is that the polymer can be described as a series of spherical blobs of diameter $\sim d$, monomers within the blobs follow a (three-dimensional) excluded volume random walk, the blobs themselves follow a two- or one-dimensional excluded volume random walk in a nanoslit or nanochannel, respectively, and hydrodynamic interactions are screened over a distance $\sim d$. The confined end-to-end length is then given by $N_b^{\nu}\cdot d$, where N_b is the number of blobs, and ν is the excluded volume random-walk exponent equal to $3/(n+2)$ in n dimensions ($n \leq 4$). Since the blob size scales with the contour length per blob (L_b) according to $d \approx L_b^{3/5}(pw)^{1/5}$, we find:

$$R_{chan} \approx N_b^{\nu}d \approx (L/L_b)d \approx (pw)^{1/3}d^{-2/3}L \quad (2)$$

$$R_{slit} \approx N_b^{\nu}d \approx (L/L_b)^{3/4}d \approx (pw)^{1/4}d^{-1/4}L^{3/4} \quad (3)$$

We see, interestingly, that the polymer length within a nanochannel scales linearly with contour length (useful for mapping positions along DNA as will be discussed later). Since hydrodynamic interactions are screened between blobs, the friction for confinement in either a chain or slit is given by the product of the number of blobs and the friction per blob:

$$\zeta \approx (L/L_b)d \approx (pw)^{1/3}d^{-2/3}L \quad (4)$$

where the blob model assumes that the friction per blob scales as d. Diffusivity is inversely proportional to this friction as given by Einstein's relation. To determine expressions for the longest relaxation time we first need to know the effective spring constant for confinement in a channel or slit, which can be found by taking the second derivative of the confined free energy with respect to the length evaluated at the equilibrium slit or channel length. It has been shown within the blob model that the elastic force to stretch a polymer in a channel‡ is proportional to $(R_{chan}d)^{-1}$, and in a slit to R_{slit}^{-2}. We note that the literature contains varying Flory type expressions for the free energy of confinement that are not all consistent with these expressions. We can now write expressions for the longest confined relaxation times as:

$$\tau_{chan} \approx \zeta R_{chan}d \approx (pw)^{2/3}d^{-1/3}L^2 \quad (5)$$

$$\tau_{slit} \approx \zeta R_{slit}^2 \approx (pw)^{2/3}d^{-7/6}L^{5/2} \quad (6)$$

Odijk has developed a reflecting rod theory[28] to account for strong confinement with $p \gg d$ where excluded volume effects are no longer as important as the intrinsic rigidity of the molecule. In this limit, the polymer segment between deflections may be thought of as a rigid rod with length $\lambda \approx p^{1/3}d^{2/3}$, and the polymer consists of L/λ rods. The extended length of the polymer is given by the projection of λ along the axial channel direction times the number of rods. Assuming that the

‡ See the note after equation III.10 in ref. 26 for more details as to the difference. The same elastic term has been found in a renormalized free energy of confinement approach.[59]

deflection angle of the rod with respect to the wall is small, we can write the polymer length as:

$$R_{\mathrm{chan}}^{\mathrm{rod}} \approx (L/\lambda)\lambda\cos\theta \approx L(1 - \alpha d^{2/3}p^{-2/3}) \quad (7)$$

$$R_{\mathrm{slit}}^{\mathrm{rod}} \approx L[1 - \beta(d_1^{2/3}p^{-2/3} + d_2^{2/3}p^{-2/3})] \quad (8)$$

where α and β are numerical factors calculated to be 17% and 9.1%, respectively,[29] and d_1 and d_2 are the confining slit dimensions with $p \gg d_1,d_2$. The free energy of confinement is simply given by the number of rods times the thermal energy. Therefore, the spring constant scales as $pd^{-2}L^{-1}$. The friction is given by the hydrodynamic interaction of a rod with the channel boundary and scales[30] as $L/\ln(d/w)$, again since d sets the length scale over which the interactions are screened. Consequently, the longest relaxation time is found to be:

$$\tau_{\mathrm{chan}}^{\mathrm{rod}} \approx \zeta/k \approx p^{-1}d^2L^2/\ln(d/w) \quad (9)$$

We note that the longest relaxation time in the blob regime monotonically increases as the channel diameter gets smaller, while in the reflecting rod regime the relaxation time decreases for decreasing diameter (above an unphysical cutoff).

B.3 Electric double layers and DNA electrophoresis

We briefly review some electrostatic concepts relevant for understanding nanofluidic systems containing DNA molecules. A large charged molecule in an ionic solution distorts the distribution of ions in its vicinity. Counterions form a permanently adsorbed Stern layer immediately surrounding the molecule and beyond this a diffuse layer where they remain mobile. The combination of these layers is termed the electric double layer. The distance over which the Stern layer forms is given approximately by the Bjerrum length, which relates electrostatic repulsion to thermal energy and is approximately 0.7 nm in water at room temperature. The distribution of the surrounding ions is given by the Poisson–Boltzmann equation whose general solution is termed the Gouy–Chapman model and linearized solution for small potentials ($\sim$50 mV at room temperature) is given by Debye–Huckel theory. In the latter, the potential is exponentially screened from its value on the surface of the molecule over a characteristic distance termed the Debye length, given by:

$$\kappa^{-1} = \sqrt{\frac{\varepsilon_0\varepsilon_{\mathrm{b}}kT}{2e^2z^2n_{\mathrm{b}}}} \quad (10)$$

where ε_0 is the vacuum permittivity, ε_{b} the fluid dielectric constant, k is Boltzmann's constant, T the temperature, e the electron charge, z the ion valence, and n_{b} the number of ions per unit volume. The Debye length ranges from 10 to 1 nm for respective concentrations of 1 and 100 mM.

Following the discussion in ref. 31, we now consider the application of a uniform external electric field that exerts a force on the molecule and also exerts a force on the mobile counterion cloud of thickness κ^{-1} surrounding the molecule. Momentarily neglecting the influence of this counterion cloud, the molecule feels a hydrodynamic drag force from its motion through the viscous solution. Additionally, then, the counterion cloud interacts hydrodynamically with the molecule as the cloud is dragged in the opposite direction. Simple solutions for the molecule's mobility may be found for the cases where the Debye length is much larger or smaller than the molecule's size. In the former case, the mobility, for a sphere of radius R and charge Q for example, is given by $\mu = Q/(6\pi\eta R)$, where η is the viscosity. When the Debye length is much smaller than the particle's size, however, Smoluchowski[32] has found that the mobility is given by $\mu = \varepsilon_0\varepsilon_{\mathrm{b}}\zeta/\eta$, where ζ is the potential approximately at the interface between the Stern and diffuse layer. In this limit, relevant for the electrophoresis of DNA molecules, the long-range hydrodynamic interactions of the counterions cancel those of the molecule, resulting in free-draining behavior where mobility is surprisingly independent of size and conformation. Consequently, large DNA molecules cannot be separated in free solution under an applied field.

The discussion thus far concerning the formation of an electric double layer also applies to a charged boundary surface in contact with the solution. We often fabricate nanochannels using a fused silica substrate that has a surface charge density of -100 mC m^{-2} in a 1 mM buffer. Under the application of an electric field, a plug-like electroosmotic flow with shear in the diffuse layer is advected toward the cathode due to the excess of counterions within κ^{-1} of the walls. This flow opposes the electrophoretic motion of DNA molecules. Also note that it is possible for the electric double layers to overlap in channels or slits with $\kappa d \approx 2$.

C. Fabrication

In this section, we outline the most widely used methods for constructing nanoslits, channels, and pores, noting relative advantages and difficulties associated with each. We then discuss some basic experimental techniques for measuring properties of DNA molecules confined within such systems. We do not intend to provide a comprehensive overview of nanofabrication methods and literature but instead reference papers illustrative of a given technique.

Nanofluidic devices are typically constructed using silicon or glass-like substrates. The most common glass-like substrates are borosilicate (Pyrex) and fused silica, an amorphous form of quartz. These materials may be controllably etched, either chemically or *via* high-energy ions from a plasma *via* reactive ion etching. They result in negative surface charge densities upon exposure to water which serves to limit DNA surface adsorption. After a pattern is etched into the substrate, the fluidic system must be enclosed. This is often accomplished by bonding another wafer anodically (for silicon–glass interfaces) at high potentials or by thermal fusion bonding above the glass transition temperature (for glass–glass interfaces). Mao and Han[33] have characterized the bonding process in the formation of 25 nm deep nanoslits with aspect ratios (depth to width) as low as 0.0005. Glass substrates offer benefits over silicon for electrophoretic DNA transport since they are non-conductive and for single molecule fluorescent experiments since they are optically transparent. Fused silica has lower autofluorescence than Pyrex making it ideal for fluorescent experiments limited in signal to noise ratio (*e.g.*, single molecule experiments using short DNA molecules).

Since slits require nanometre precision in the single dimension of depth only, they may be fabricated *via* standard photolithographic processes. Photolithography involves the use of light (typically ultraviolet) to expose a pattern in a photosensitive chemical spun over a wafer, where a mask is usually placed between the source and the wafer to define the pattern. The minimum feature size is limited by the diffraction of light (roughly by the ratio of the wavelength to the numerical aperture in a projection system). There are a large number of photoresists available that offer excellent selectivity in etch rates relative to silicon or glass substrates. Due to its prominence in the fabrication of transistors for computers, photolithography is quite capable of high throughput pattern definition over wafers.

Electron beam (e-beam) lithography is a conceptually similar process using a focused beam of electrons to chemically alter a resist *via* energy loss through ionization.[34] Typical e-beam machines generate electron energies between 10 and 100 keV corresponding to sub nm de Broglie wavelengths. However, the feature resolution is limited to critical dimensions of approximately 10 nm due to scattering in the resist as opposed to diffraction. E-beam lithography is often used for the fabrication of nanochannels and pores, though it is a time consuming and expensive technique not well suited for exposing large areas across an entire wafer. Focused ion beam (FIB) lithography, whereby a focused beam of ions (typically Ga) physically sputter neutral and ionized substrate atoms upon impact, has also been used to fabricate nanochannels[35] and pores.[36] This method is quite versatile since it can be used to etch, image, and deposit films in conjunction with precursor gases (similarly to chemical vapor deposition). However, it is more useful for prototyping than for patterning large areas.

To address the limitations of e-beam and FIB for rapid large scale patterning, Chou and colleagues[37,38] invented nanoimprint lithography whereby a mold with nanostructures created using e-beam (or interference) lithography is pressed into a thin resist spun on a substrate and raised above its glass transition temperature. After cooling the resist, the mold is removed and the resist is anisotropically etched to remove the residual resist within the compressed regions. This process results in the creation of a template that can be used repeatedly to quickly generate nanoscale features across a wafer. Cao *et al.*[40] combined this technique with non-uniform sputtering of silicon dioxide to narrow and seal millions of channels with dimensions 10 by 50 nm across a 100 mm wafer. Liang *et al.*[39] recently combined nanoimprint lithography with a novel mold fabrication method based on crystallographic anisotropic etching of silicon combined with conformal silicon nitride deposition as depicted in Fig. 2. This non-lithographic technique results in an atomically smooth mold capable of being transferred to a UV-curable material layer resulting in smooth nanochannels 11 nm wide and 1.5 cm long. To transfer the pattern to an underlying substrate (though the pattern in the mold itself can be used for nanochannels) requires a single reactive ion etch that can result in a roughened channel surface (as in typical e-beam fabrication). Xia *et al.*[41] developed a new method to seal and shrink sub-10 nm trenches made by NIL in silicon using a 20 ns ultraviolet laser pulse to melt and flow a thin surface layer. The authors also thermally oxidized the silicon in order to reduce the width of the trenches and to make them optically transparent for subsequent DNA analysis.

Instead of etching a structure and bonding a wafer to create a nanoaperture, the use of a sacrificial material has proven very successful. This process consists of depositing and patterning a sacrificial layer of material onto a substrate, depositing a capping layer that covers and encloses the sacrificial layer, and finally removing the sacrificial layer. The resultant self-sealed channel is constructed with a fixed depth based on the controlled deposition of the sacrificial layer. Devices have been made incorporating polysilicon,[42] polycarbonate,[43,44] or polynorbornene[45] as the sacrificial material which can be removed chemically or by disintegrating the polymer at elevated temperatures. The capping layer is typically sputtered silicon oxide or chemical vapor deposited oxide or nitride. Electrospun polymer fibers have also been used as sacrificial materials for non-lithographic nanochannel fabrication.[46] Other unconventional approaches have relied on nanosphere lithography[47] or mechanical cracking[48] of oxidized polydimethylsiloxane (PDMS) for the fabrication of

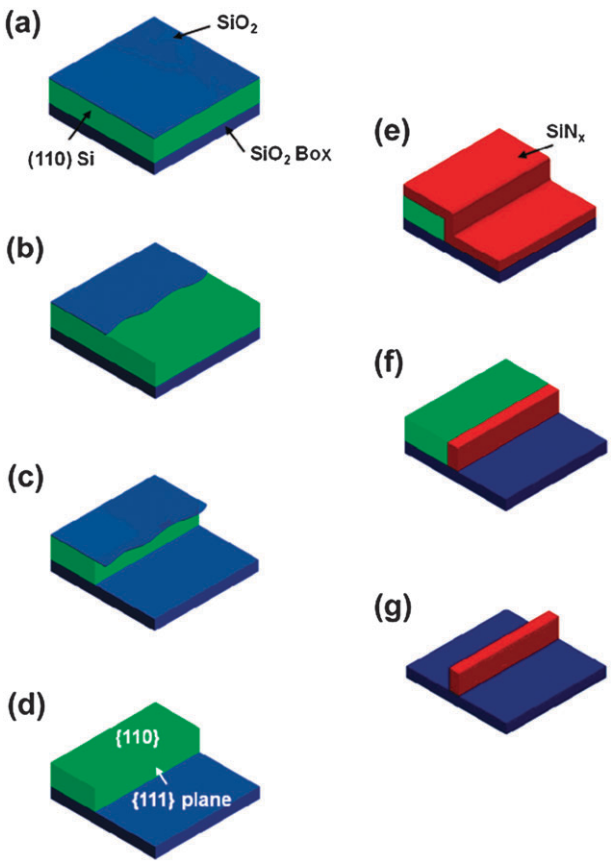

Fig. 2 Fabrication schematic of nanoimprint lithography mold for a long atomically smooth nanofluidic channel. (a) Thermal oxidation to form SiO_2 on a (110) Si surface. (b) Photolithography and patterning of a large rectangle with a long edge aligned to the {111} axis. (c) Crystallographic anisotropic etching of (110) Si. (d) Removal of the SiO_2 mask. (e) Conformal deposition of Si_xN_y. (f) Reactive ion etch of Si_xN_y on top of Si mesa but not the sidewall. (g) Removal of (110) Si to create a free-standing Si_xN_y wall. Reprinted from ref. 39 with permission from © American Chemical Society (2007).

closed fluidic channels in which DNA molecules were introduced. While PDMS structures are useful for rapid prototyping, their inherent flexibility makes them suboptimal for measurements that depend on precise knowledge of the confining boundary dimensions.

In addition to the precise fabrication methods listed, a few rougher methods are often employed outside of a cleanroom to produce useable fluidic devices for DNA manipulation. For example, one needs to add a macroscopic reservoir connected to the fluidic channel for the introduction of DNA molecules. Our group commonly uses a glass bead abrasive unit (sand blaster) to punch a millimetre-sized hole through a fused silica wafer with features etched on the opposite side (after protecting the wafer with thickly spun photoresist). After thermal bonding to seal the channel, we use ultraviolet curable glass epoxy to adhere the bottom half of a pipette tip around the hole for use as a reservoir. Wetting the fluidic system can also pose a difficulty depending on the internal dimensions and hydrophobic nature of the substrate. Riehn and Austin[49] have developed a supercritical wetting technique using a pressurized cell to fill arbitrarily shaped nanofluidic structures in a matter of hours. Many of the experiments reviewed use an intercalating dye such as YOYO-1 for fluorescent imaging of individual DNA molecules. The literature trail concerning the influence of such intercalating dyes on the physical characteristics of DNA molecules that experimenters often wish to measure is slightly convoluted. However, it is generally accepted that TOTO and YOYO dyes increase the contour length by 30–35% for staining at the maximum ratio of 4 : 1 base pair to dye molecules.[50] It is also often assumed that the persistence length is increased by the same amount but an optical-tweezer experiment has measured a much lower value with YOYO-1 than for the unstained persistence length.[51] Additionally, an oxygen scavenging molecule such as β-mercaptoethanol at a few percent (v/v) is often added to the DNA buffer to reduce photodamage.

D. DNA manipulation

The first elegant demonstration of the dramatic effect that confinement has on DNA dynamics was based on electrophoretically elongating DNA molecules around fabricated pillars in nanoslits of various heights.[52] At a given field strength, measured by tracking the velocity of undeformed molecules away from the pillars, molecules in shallower slits extend more than in deeper slits. This extension results from an increased hydrodynamic drag in shallower slits due to the screening of hydrodynamic interactions over the length scale of the slit depth, resulting in nearly free-draining behavior at the shallowest depths. This experiment also corroborated the somewhat non-intuitive electrohydrodynamic equivalence theory[53] that a charged polymer held immobile in a uniform electric field extends the same as in a hydrodynamic flow of uE, where u is the electrophoretic mobility. Clear confirmation that the drag depends on slit depth was demonstrated by plotting the contraction of the molecules as a function of time in three slit depths ranging from 90 nm to 5 μm after they unhooked from the posts.

D.1 Quantitative comparisons with confined polymer theory

Several experiments subsequently attempted to quantitatively investigate the predictions of confined polymer theory in nanochannels. Guo *et al.*[54] first measured the equilibrium extension of individual DNA molecules in nanochannels fabricated by nanoimprint lithography. They found increased extension for decreasing nanochannel diameter but did not make detailed comparisons to theory. Two experiments from the Austin group similarly observed the equilibrium extension and fluctuations in extension of DNA molecules electrophoretically driven into nanochannels using fluorescent video microscopy.[30,55] As explained in the Theory section, according to blob theory, a DNA molecule confined to a nanochannel with a diameter smaller than its bulk radius of gyration and larger than its persistence length is expected to have an extended length that scales as $L/d^{2/3}$, where L is the contour length. It was first found[55] that the scaling of R_{chan} with L holds for long DNA with extended lengths up to 200 μm. In this experiment, lambda DNA molecules (48.5 kbp) were extended to approximately 35% of their 22 μm (TOTO-1 stained) contour length in 100 nm wide and 200 nm deep nanochannels.[55] Also, the authors derived an effective spring constant for the thermal fluctuations around the equilibrium length based on the free energy of confinement from the de Gennes theory. This leads to the prediction that the standard deviation of the extended length scales as $L^{1/2}$, which was also corroborated by making statistically independent measurements of the length of a given molecule over time for different sized molecules.

Reisner *et al.*[30] continued this analysis by measuring that the extended length of lambda DNA scales with the channel diameter as $d^{-0.85\pm0.05}$ in nanochannels ranging from approximately 60 to 500 nm, in disagreement with the predicted exponent of 2/3. Fig. 3 displays the extended length of lambda and T2 (164 kbp) molecules in nanochannels of varying diameter. Additionally, by fitting the autocorrelation function of the extended length as a function of time to an exponential, the scaling of the DNA relaxation time as a function of nanochannel diameter was also measured. The relaxation time scaled with channel diameter with an exponent of -0.9 ± 0.4 for channels with diameters larger than 140 nm and beneath this cutoff decreased with decreasing channel diameter as shown in Fig. 4. Again the exponent disagrees mildly (at the one and one-half sigma level) with the de Gennes prediction of 1/3, and the qualitative change in behavior at a confining diameter of approximately twice the persistence length is attributed to a transition to the Odijk regime where the relaxation time is expected to scale according to eqn (9). Persson *et al.*[57] have also measured the scaling of lambda and circular charomid DNA extension with channel diameter using a tapered nanochannel design so that a given molecule can easily be measured at different diameters while ensuring identical solvent conditions. They found the same scaling for lambda with channel diameter as Reisner *et al.* but discovered that circular DNA scales more weakly with diameter with an exponent of 0.65 ± 0.01, in agreement with blob theory prediction. The authors surmise that excluded volume interactions may be responsible for the difference due to the

approximately doubled contour density for circular compared to linear DNA. However as the extension at a given confinement for circular DNA is found to be approximately 5% less than that for linear DNA, it seems that more experiments will be needed to sufficiently probe this difference.

Reccius *et al.*[58] investigated for the first time the expansion of initially compressed DNA molecules in nanochannels using blob theory constructs. DNA molecules were driven into 140 nm diameter nanochannels containing constrictions at random positions due to fluctuations during the fabrication process. The expansion of the molecules as a function of time was derived after constructing an expression for the free energy of confinement as a function of extended length, based on Flory and blob theory. By measuring the time constant of expansion, a value for the persistent length of different sized DNA molecules was obtained, which differed with respect to molecular length and the expected value from the literature. The discrepancy was conjectured to result from differing initial compressions, by possible DNA kinking, or by the inability of the equilibrium theory to account for the non-uniformity of the compressed state. Subsequent formulations based on scaling analysis and molecular dynamic simulations have been derived for the force induced deformation of self-avoiding chains inside cylindrical nanopores.[59]

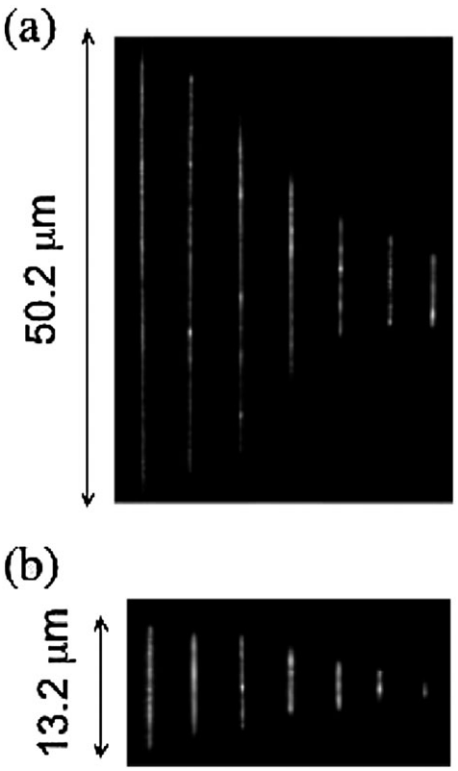

Fig. 3 (a) Equilibrium length of fluorescently stained T2 DNA molecules in nanochannels with an average diameter of approximately 35, 70, 80, 135, 185, 360, and 440 nm, respectively, from left to right. (b) Equilibrium length of lambda DNA molecules in the same channels. Reprinted from ref. 30 (http://prola.aps.org/abstract/PRL/v94/i19/e196101) with permission. Copyright 2005 by the American Physical Society.

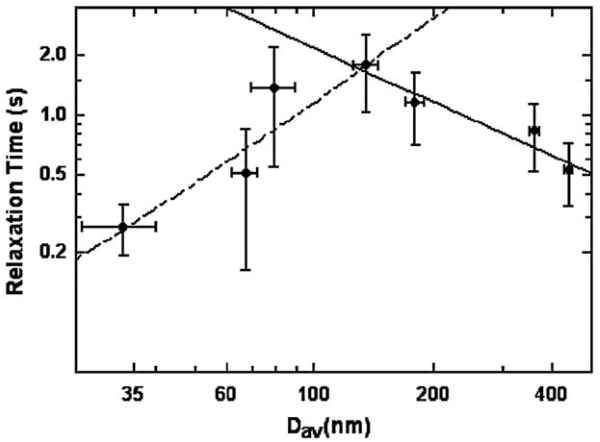

Fig. 4 Log–log plot of lambda DNA relaxation time as a function of the average nanochannel diameter. A best power-law fit to the data for channels larger than 140 nm (bold curve) and a fit to the rigid rod model of eqn (9) for smaller channels (dashed curve) are overlaid. Reprinted from ref. 30 (http://prola.aps.org/abstract/PRL/v94/i19/e196101) with permission. Copyright 2005 by the American Physical Society.

In contrast with the nanochannel experiments, quite a number of different groups have made quantitative (or semi-quantitative) comparisons between blob and rod theory predictions and measurements in nanoslits. Further, as the groups have focused on different observables, the results are still somewhat contradictory. The Doyle group has established itself as the leader in the field with several groundbreaking papers published over the last five years using epifluorescent video microscopy to observe individual DNA molecules. We first summarize the results that have been obtained by this group before reviewing competing measurements in nanoslits.

Balducci *et al.*[56] originally measured the equilibrium scaling of both diffusivity and molecular weight with nanochannel depth h for confinements in the range of $0.4 < R/h < 14$, where R is the DNA bulk radius of gyration (approximately 700 nm for lambda DNA[60]). A summary of their image analysis technique to measure self-diffusion coefficients for a 2λ-DNA concatamer in a 545 nm slit is shown in Fig. 5. They observed that diffusion scales more weakly with depth than indicated by blob theory (an exponent of 0.55 ± 0.05 for lambda DNA *versus* the 2/3 prediction) and that diffusion scales inversely proportional to molecular weight for channels with $h < R$, which indicates that hydrodynamic interactions are screened over the DNA coil length. They also reported no change in the scaling of diffusivity for channels with depths that approach the DNA persistence length, concluding that there must be a broad transition in nanoslits between blob and reflecting rod theory. Brownian dynamic simulations by Jendrejack *et al.*[61] and mean field numerical calculations by Harden and Doi[62] both find that the diffusivity scales less strongly with height than given by blob theory. This work was followed by a paper from Hsieh *et al.*[60] where the equilibrium diffusivity and rotational relaxation time were measured as a function of both molecular weight and depth in nanoslits with depths down to approximately 100 nm.

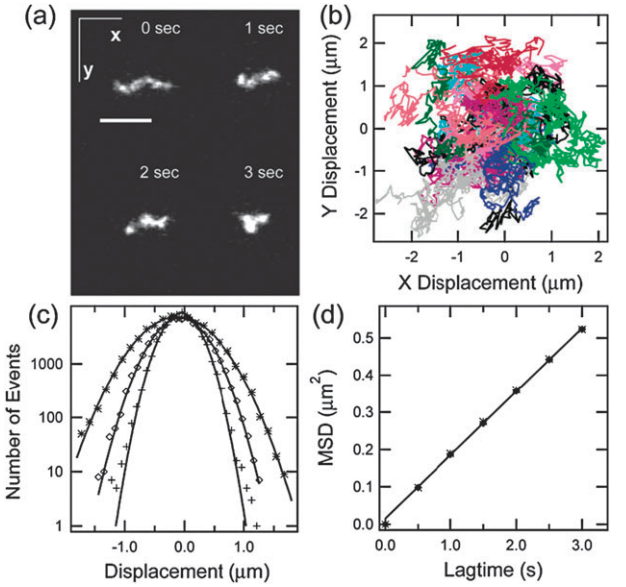

Fig. 5 Summary of diffusion image analysis for 2λ-DNA in a 545 nm deep nanoslit. (a) Time-series images of DNA molecule in slit (scale bar is 5 μm). (b) Center of mass trajectories for 28 molecules. (c) Probability density functions (not normalized) for trajectories at lagtimes of 0.33 (+), 0.66 (◇), and 1.23 (*) seconds with respective fits to a Gaussian curve (solid lines). (d) Mean-squared displacement (◇) and the variance of the probability density function (*) as a function of lagtime. Reprinted from ref. 56 with permission from © American Chemical Society (2006).

Hsieh *et al.*[60] confirmed the previous diffusivity measurements and determined from fitting the rotational autocorrelation function to an exponential that the relaxation time scales with depth to the power -0.92 ± 0.08 for lambda DNA, in contrast with the blob theory prediction of $-7/6$. The authors go to considerable length in separating out the various assumptions of the theory, by measuring how the product of diffusion and relaxation time scales with depth, to arrive at the conclusion that blobs do follow two-dimensional self-avoiding walks but are partially draining, respectively, in agreement and disagreement with the theory. They also mention that they attempted to measure the relaxation time using the autocorrelation of the observed length but found this method biased by photobleaching effects and by needing an accurate estimate for the mean stretch. The authors found that their results for relaxation time as a function of confinement do not agree with those found by Bakajin *et al.*[52] in the experiment already mentioned. In another follow up paper, Balducci *et al.*[63] solved this apparent discrepancy by discovering that there are two distinct relaxation regimes at different extensions during relaxation in nanoslits. As stated, Bakajin *et al.* measured relaxation after initially stretching the DNA around pillars (which Balducci repeats) while Hsieh *et al.* measured the equilibrium rotational relaxation time. Balducci finds that an initially stretched polymer relaxes by increasing the size of its tension blobs (similarly to a polymer in bulk) with a reduced drag coefficient due to confinement. However, when the blobs reach the size given by the depth of the channel, the polymer relaxes by rearranging the blobs as a two-dimensional self-avoiding chain. In the first regime, the relaxation time scales with the channel depth to the $-1/2$ power while in the second regime, the same scaling holds as was found by Hsieh.

We note that two separate experiments reported that blob theory correctly predicts the scaling of diffusivity with channel depth[64] and scaling of extension and relaxation time with molecular weight[65] (both using fluorescent video microscopy) probing confinements up to $R/h < 7$ and 14 respectively. However, the measured relaxation times reported[65] in slits with similar depths to those studied by Hsieh *et al.* differ by approximately a factor of four. Also, Strychalski *et al.*[66] measured *via* fluorescent video microscopy the scaling of diffusivity and molecular weight with channel depth, probing confinements between $1/2 < R/h < 29$ in an attempt to also probe the alluded to broad transition expected between blob and reflecting rod theory. These authors found that diffusion scales with height to the power -0.47 ± 0.05 (quite similarly to the results of Balducci and Hsieh) in disagreement with blob theory in nanoslits down to approximately 30 nm in height, well below the expected transition to reflecting rod theory. However, no change in this scaling was evident at these shallow channel depths. The authors also found an anomalous value for diffusion in a 25 nm deep slit that did not match either theory where the diffusional motion was preferentially directed perpendicular to the entropic barrier between the nano- and microchannel region of the device. These measurements were thought to be influenced by surface roughness.

In a further twist, Bonthuis *et al.*[67] measured the scaling of extension and relaxation time of lambda DNA molecules as a function of channel depth in nanoslits with similar confinements as those used by Strychalski *et al.* However, Bonthuis *et al.* observed a strong discontinuity in the scaling of both variables at $h \approx 100$ nm which the authors attribute to the transition from the de Gennes to Odijk regime. Strikingly, the extension beyond this transition channel height plateaus, in disagreement with the prediction, and the relaxation time decreases by a factor of 2 for a factor of 3 decrease in channel height, while the theory predicts a much milder, ln (h), decrease of 35%. The absolute value of the relaxation time found by Bonthuis *et al.* in a $\sim$100 nm deep slit is about a factor of 3.5 less than that found by Hsieh for a similar slit depth, though much of the difference can be explained by a different fluorescent dye staining ratio, ionic strength, and buffer viscosity.[68] It is also claimed that the extension and relaxation time scaling in the de Gennes regime agrees with the theory predictions of $1/4$ and $-7/6$, respectively, within the experimental precision (though this precision is unstated), also in contrast to the Hsieh relaxation time result. Bonthuis *et al.* measured the relaxation time by fitting an exponential to the autocorrelation of the extension, a possible source of the different values obtained. A recent result[69] also measures a plateau in the extension of lambda DNA in nanoslits between the heights of 20 and 100 nm. We note that it will remain rather difficult to experimentally quantify the scalings of extension or relaxation time in the Odijk regime simply due to the gradual changes predicted over heights that span less than one decade. In other words, a power-law fit may yield a reasonable exponent (with small error) but that does not necessarily mean that the power-law assumption is validated.

D.2 Ionic effects on conformation and dynamics

As stated in the Theory section, the equilibrium extension of DNA is determined by the balancing of an entropic compressive force and a repulsive electrostatic force between segments separated a long distance along the contour. Several groups have attempted to quantify the latter effect by varying the ionic concentration of the DNA solution. Since the Debye length scales as $I^{-1/2}$, where I is the ionic strength of the electrolyte, reducing the salt concentration should lead to charges being screened over longer distances and hence increased excluded volume effects and larger extensions in nanofluidic devices. The situation is complicated, however, since the persistence length of DNA also depends on the ionic concentration according to the formula of Odijk,[70] and Skolnick and Fixman[71] (OSF):

$$p = p_0 + \frac{1}{4 l_B \kappa^2} = \left(p_0 + \frac{0.0324 M}{I}\right) \text{nm} \qquad (11)$$

where p_0 is the intrinsic (non-electrostatic) persistence length, l_B is the Bjerrum length (0.7 nm in aqueous solution at room temperature), and κ is the inverse Debye screening length.

It was reported[72] that the scaling of persistence length with ionic strength sufficiently explains observed extensions of DNA molecules in PDMS nanoslits of height 100 nm and width 1 μm over a range of salt concentrations varying from approximately 0.1 to 10 mM. In this experiment, the DNA extension plateaus at approximately 50% of its contour length,[72] similar to extensions in 35 nm nanochannels with fifty times larger ionic strength conditions.[30] However, the authors did not consider changes to the long-range excluded volume interactions due to an increase in the effective diameter of the DNA at low salt concentrations. This additional effect was considered by Reisner *et al.*,[73] who used the following formula for the effective width as a function of Debye length as calculated by Stigter:[74,75]

$$w = \frac{1}{\kappa}\left(0.7704 + \log\frac{2\pi \nu_{\text{eff}}^2}{k_B T \varepsilon \varepsilon_0 \kappa}\right) \qquad (12)$$

where ν_{eff}^2 is an effective line charge of the DNA that depends on the bare line charge and ionic strength, $k_B T$ is Boltzmann's energy, and ε is the dielectric constant of water. Reisner *et al.* were able to describe the fractional extension of DNA in nanochannels of 50, 100, and 200 nm nanochannels varying the ionic concentration between 10–200 mM based on the de Gennes blob expression with both the width and persistence length as a function of ionic strength as given by eqn (11) and (12). Further, Reisner *et al.* found that using the persistence length dependence on ionic strength alone fails to account for the variation in fractional extension, which ranges from 0.60 to 0.85 in the 50 nm channel at the upper and lower concentrations listed respectively. Reisner *et al.* also plot the observed variation in extension with the prediction from Odijk *et al.*[72] (which only has persistence length ionic strength dependence), and conclude that it cannot accurately describe the data. Similarly, Hsieh *et al.*[76] use a blob model with an effective width and persistence length that depend on ionic strength as given by the previous formulas (and additionally a persistence length that depends inversely on the square root of the ionic strength) to explain the diffusion and rotational relaxation times of DNA in nanoslits as a function of ionic strength. Varying the salt concentration between 2 and 170 mM, they find that the width dependence, representing long-range excluded volume interactions, is mainly responsible for predicting the roughly two and four-fold variation of the diffusion and relaxation time respectively. The authors were careful to account for changes to the viscosity due to the ionic concentration as well.

To significantly confuse matters yet again, Zhang *et al.*[77] also measured the extension of DNA in 300 nm deep and 150–300 nm wide PDMS channels as a function of salt concentration ranging from 0.3 to 30 mM. The observed extensions in their narrowest channels agree well with those found in Reisner's largest channels. However, their interpretation of the cause differs. They treat the DNA width and persistence length as having the same electrostatic dependence within the blob model, but they derive a different expression for the fractional extension based on using the full Benoit–Doty[78] equation for the unswollen radius of gyration of blobs within the channel. They argue that there are a relatively small number of persistence lengths within each blob and that the inclusion of excluded volume effects are basically not necessary to fit their data. They find that the excluded volume parameter[71] is between 0.2 and 0.5 for all nanochannels and salt concentrations investigated, implying that the blob radius of gyration follows a theta solvent scaling with blob contour length. Unfortunately, the derived expression for the extension must be solved numerically§ and cannot be easily compared to the scaling of extension *versus* channel diameter previously also measured by Reisner *et al.* (and discussed in the previous section). We note that Balducci[56] *et al.* raised a similar point concerning the ability of the blobs to follow excluded volume scalings in nanoslits, estimating the crossover height for blobs to be swollen at ~800 nm. Odijk has also theorized a crossover region[79] within the classic blob regime where excluded volume interactions become important for channels with diameter larger than $p^2/w \approx 500$ nm (where the numerical value is given at high salt concentration). If one uses the theta solvent Flory radius of gyration $R_0 \approx L^{1/2}$ then the fractional extension and relaxation time of DNA should both scale with the inverse power of nanochannel diameter, more closely in line with the experimental results obtained by Reisner *et al.*[30] But, as previously mentioned, Hsieh *et al.* were quite careful to separately examine predictions of blob theory and found the assumption of the monomers to follow a three-dimensional self-avoiding walk (3/5 exponent) to accurately predict the data in slits down to 100 nm in height.

In conclusion, the experimental evidence is quite clear that both conformational and dynamical properties of DNA molecules confined to nanofluidic structures have an important dependence on ionic concentration. However, this dependence results in changes of fractional extension or relaxation time that are approximately a factor of two or three over two decades change in salt concentration. Thus it seems that

§ For channel diameters larger than 100 nm, we found that the fractional extension scales roughly inversely with the diameter using expressions (1) through (4) of ref. 77.

whether the cause of this change is mainly due to electrostatic dependence on DNA width or persistence length is still a matter for some debate, though the results from the Doyle group suggest the width dependence to be the most important factor (having also validated the importance of excluded volume effects for monomers within blobs).

D.3 Entropic effects

We have already discussed the entropic elasticity of DNA due to the Gaussian probability distribution for its end-to-end vector. There is a distinct entropic force experienced by a polymer subject to a gradient in its confining geometry. When a polymer is positioned across a boundary region where the number of available molecular configurations changes, the entropy and free energy also change across the boundary, leading to a localized force that acts to move the polymer to the area with larger configuration space. Such effects due to entropic trapping were theorized to explain anomalous mobility differences observed for the motion of DNA in gel electrophoresis.[80–83] We will discuss experiments that have measured entropic forces on confined DNA in this section, and discuss the application of using these forces for DNA separation in the following. We note, for now, that Han and Craighead were the first to observe entropic forces in precisely defined nanofluidic structures.[84]

The first observation of polymer displacement due to a confinement dependent entropic force was reported[85] using a 60 nm high slit region filled with 35 nm diameter pillars constructed using a sacrificial technique. DNA molecules were electrophoretically positioned across the boundary of the pillar and pillar-free regions. When the electric field is removed, the DNA molecules recoil from the low-entropy region (containing pillars) to the high entropy region where they have more configurational freedom. Assuming that the entropy in the pillar-region depends only on the length of the DNA molecule in that region, and that the hydrodynamic friction coefficient is proportional to that length (since the shallow slit screens these interactions over longer lengths), the length of the molecule in the low-entropy region as a function of time may be written as:

$$L = \sqrt{-\frac{2f}{\rho}(t - t_0)} \qquad (13)$$

where t_0 is the time the molecule completely recoils, ρ is the specific drag, and f is the length independent entropic force. This equation proves to effectively model the recoil data, which allows for a lower bound estimate of the entropic force of $f \geq 6$ fN, once the drag is estimated from first principles. It is notable that this force is below the resolution of optical-tweezer force measurements.[57] Also the force observed is distinct from entropic elasticity where the recoil has been shown to be initially rapid and gradually slowing,[86,87] as opposed to entropic recoil that follows the opposite behavior.

Entropic confinement forces were subsequently examined in more detail[9] by positioning DNA molecules at the interface between a nanochannel of diameter 100 nm and a $\sim$10 μm wide nanoslit. The basic process where a molecule at equilibrium inside the nanochannel is transported to the boundary and recoils was observed and compared well to the same model described in eqn (13). Additionally, molecules were observed to enter the nanochannel under the application of an electric field in a folded configuration where a portion of the molecule distinct from the ends enters first. These molecules were observed to unfold while recoiling. Molecules were stretched while entering the nanochannel due to a combination of electrophoretic and entropic forces pulling in opposite directions and observed to elastically contract to their equilibrium lengths. Finally, molecules partially driven into the nanochannels were observed to recoil entropically while contracting as illustrated in Fig. 6. A so-called intensity time trace depicting the intensity of the DNA molecule projected along the nanochannel axis as a function of time shows the contraction, entropic recoil, and combination processes in Fig. 7. Mannion *et al.* found that f/ρ was three times larger than the value reported in ref. 85, presumably due to the larger entropic force from confinement in nanochannels as compared to pillars. The measured entropic force was found to be 220 ± 40 fN, after an estimate was obtained for the hydrodynamic friction coefficient.

Another entropic force was observed for folded DNA molecules positioned within nanochannels[88] of diameter 140 and 180 nm. By selectively applying an electric field while molecules diffuse near an entrance to a nanochannel, it is possible to force the molecule into the channel in a folded configuration (where a portion near the middle of the molecule enters first). These DNA molecules (of length $\sim$166 kbp) spontaneously unfold over tens of seconds. Further, it was

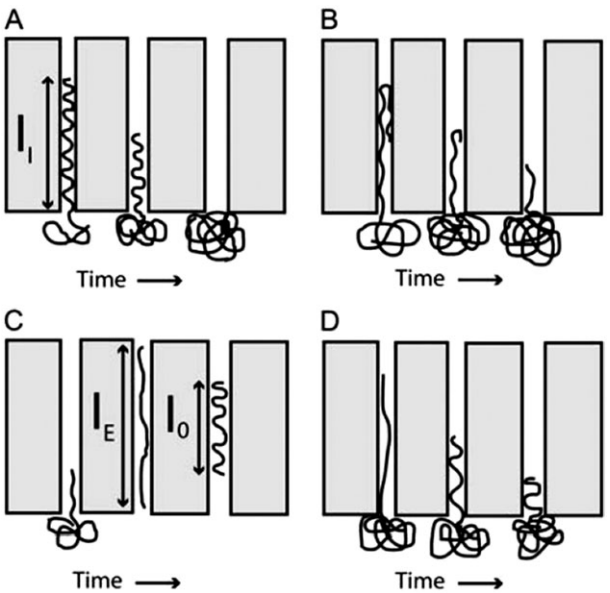

Fig. 6 Schematic representation of entropic recoiling and relaxation of DNA molecules in nanochannels. (A) Entropic recoiling of a DNA molecule from a nanochannel after the molecule has been given sufficient time to relax to its extended equilibrium extension within the channel. (B) Entropic recoiling of a molecule with a folded front end where the recoil process unfolds the molecule before it exits the channel. (C) Relaxation of an electrophoretically stretched molecule to its equilibrium extended length within a channel. (D) Recoil of a molecule driven into a channel before it has had time to relax to its equilibrium extension. Reprinted from ref. 9 with permission from © Biophysical Society (2006).

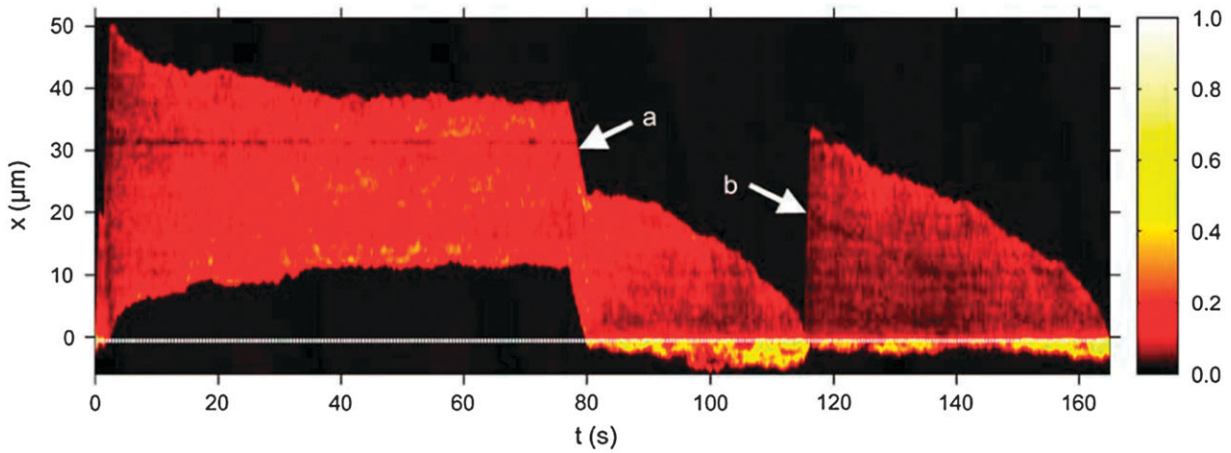

Fig. 7 Intensity–time trace of three manipulations performed with a T4 DNA molecule. The normalized intensity along the channel position is plotted *versus* time (the dotted line denotes the channel entrance). The molecule is initially electrophoretically driven into the channel, stretched, and relaxes to its equilibrium length. The molecule is moved to the channel entrance after 77 s (a) where it begins to recoil. At 115 s the molecule is driven partially back into the channel (b) and again recoils but this time before it has been given sufficient time to relax to its equilibrium length. The different profiles of the recoiling molecule are evident. Reprinted from ref. 9 with permission from © Biophysical Society (2006).

observed that the equilibrium extension per unit length for the folded portion was approximately 30% larger than the equilibrium extension for unfolded molecules, presumably due to increased excluded volume interactions for the folded portion. By numerically solving a model that accounts for the hydrodynamic friction on the upper and lower portions of the folded molecule, the estimated unfolding force was found to be approximately 20 fN, which agrees well with theoretical estimates.[89] It has also been theorized that confinement resulting in entropic self-repulsion may play a role in bacterial chromosome segregation.[4]

We note a few additional experiments concerning DNA manipulations that do not fit into the topics we have discussed thus far. Reisner *et al.* constructed periodic arrays of 100 nm deep pits etched within a larger 100 nm high nanoslit.[90] Upon entering the nanoslits, DNA molecules would self-assemble into a conformation consisting of fluctuating linker strands connected to a varying number of filled pits. The dependence on the number of filled pits and stability of the conformations was studied as a function of the periodicity of the pit spacings. Krishnan *et al.*[91,92] have observed the spontaneous stretching of DNA molecules at the sidewalls of 100 nm deep nanoslits at relatively low salt concentrations (1 mM). The counter-intuitive electrostatic attraction between the DNA and negatively charged walls is attributed to a polarization-induced force due to the spatially varying electric field at the slit edges. This phenomenon was further explored by a separate group who measured the extension of the DNA as a function of nanoslit height when confined to the slit boundary.[69] Riehn *et al.* made a nanofluidic railroad switch[93] consisting of an array of 90 nm diameter channels perpendicular to a 140 nm diameter array. DNA molecules preferentially traveled through the wide channels under the application of an external dc field (directed along the bisector of the channels) but migrated to and along the narrow channels when an ac field was added. The authors explain the phenomenon in terms of entropic and dielectrophoretic forces that can be tuned by the applied ac field.

E. DNA sorting

A substantial practical motivation for many of the previous studies of confined DNA is to learn what principles might be applied in fabricating a device capable of sorting DNA molecules by length. We have already explained in the Theory section that DNA molecules unfortunately have a free-solution electrophoretic mobility independent of length (above an experimentally determined[94] limiting length of $\sim$500 bp). The substantial time required to separate long DNA molecule (larger than 40 kbp) by pulsed gel electrophoresis makes an alternative method desirable. Nanofluidic systems offer the opportunity for separation through entropic forces, surface induced frictious forces, and through interesting interactions of charged molecules electrophoresed through overlapping electric double layers.

One of the simplest methods for sorting is to directly measure the length of individual DNA molecules. This can be done by illuminating a DNA molecule uniformly stained with an intercalating fluorescent dye and measuring the number of photons emitted in the relevant spectral band using a photodiode. Since the number of intercalated dye molecules is proportional to the contour length of the molecule, DNA length can be determined in this manner without stretching the DNA. This principle was originally demonstrated[95] in a 5 μm wide PDMS fluidic channel to size DNA fragments between 2 and 200 kbp at a throughput of 300 molecules per minute. To achieve high resolution, the laser illumination profile over the width of the channel should be uniform, only one molecule should traverse the illumination region at a time, and the channel dimensions should be reduced, thereby improving the signal to noise. These goals were realized in a device[96] with a channel 270 nm deep and 1 μm wide (constructed using a sacrificial layer). DNA molecules were sized over the same size range but smaller fragment were resolved at speeds 40 times larger than previously used.

E.1 Entropic sorting

In a series of papers, Han and Craighead *et al.* utilized the previously described entropic barrier between a nanoslit and

microslit region to trap and then temporally separate long DNA molecules.[84,97–99] They describe the counter-intuitive discovery that longer DNA escapes the entropic trap (*e.g.*, its motion is stalled for less time) than shorter DNA,[84] present a theory that describes this phenomenon and provides a good match to their observations,[97] design a separate device to utilize the entropic traps to separate DNA molecules from 6 kbp to 160 kbp in length,[99] and explore in detail the comparison between the theory and data by varying the relevant parameters of their device for optimized separation.[98] The basic design of their device is illustrated in Fig. 8. A periodic array of wide nanoslits of depth 90 nm adjoining wide microslits of depth $\sim$1 μm are fabricated on silicon wafers (subsequently oxidized), using photolithography and wet etching techniques, that are bonded to Pyrex cover slips. As DNA molecules are electrophoretically driven through the device, they are temporarily trapped at the boundary for a characteristic time before they extend a small 'beachead' portion into the nanoslit, at which point they are stretched and transported through the slit. The authors found that the trapping time can be written as the following Arrhenius-type equation

$$\tau = \tau_0 \exp\left(\frac{\alpha}{Ek_BT}\right) \qquad (14)$$

where the activation barrier is given by the exponential term, E is the electric field strength in the slit region, and is independent of length. The prefactor represents the probability to escape per unit time and depends on the number of monomers facing the boundary region and scales roughly as $1/(dR_0)$, where d is the nanoslit depth and R_0 is the bulk radius of gyration, at low electric field strength. However, the separation resolution was found to depend on the electric field strength most likely because the process of DNA relaxation between traps is unaccounted for in the model. A bond fluctuation Monte Carlo simulation was found to be consistent with the data and the observation that longer molecules escape before shorter ones due to the hernia nucleation process.[100] A device constructed based on this principal separated long DNA in 1/20 of the time needed to achieve the same resolution *via* pulsed field gel electrophoresis. Cabodi *et al.*[101] used the mechanism of entropic recoil described in Section D.3 to separate 167 from 39 kbp molecules at the boundary of a pillared region by periodically pulsing a dc electric field (at a field strength large enough to overcome the trap). After the pulse, the longer molecule that was partially inserted would recoil while the fully inserted shorter molecule remained approximately stationary.

Quite interestingly, Han and colleagues used a device with similar geometry to separate short DNA (between 50 and 800 bp) as well as denatured proteins.[102,103] The physics behind this separation scheme is based on an Ogston sieving type of entropic barrier. This barrier is due to the steric constraints that nanoslits larger than the DNA radius of gyration present by reducing configurational phase space inside the slit (*e.g.*, since molecules cannot overlap the walls only certain orientations of the short DNA molecules are allowed). It is important to note that these shorter molecules are not deformed upon entering a slit so this separation mechanism is distinct from the previously described conformational

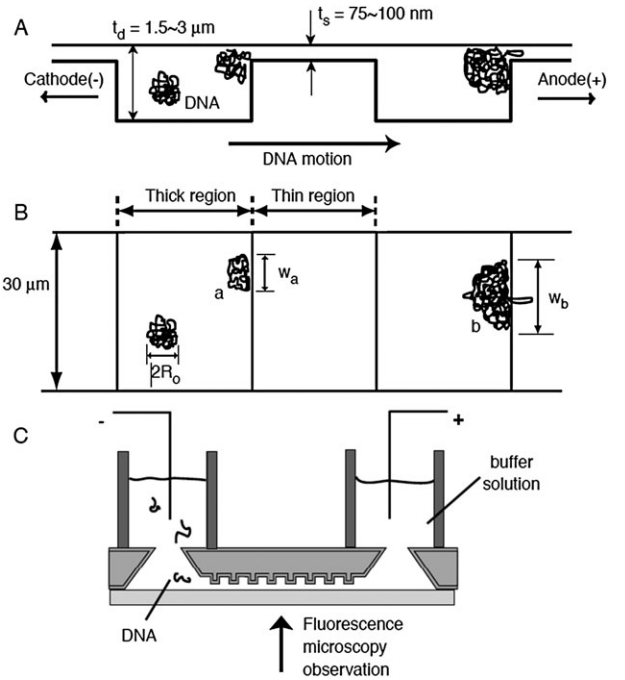

Fig. 8 Schematic representation of nanofluidic separation device containing arrays of entropic traps. (A) Side view schematic of device. Electrophoresed DNA molecules encounter entropic traps at the nanoslit entrances since their bulk radius of gyration is larger than the slit depth (t_s). (B) Top view schematic of the device showing trapped molecules whose escape rate is proportional to the length of the slit covered by the molecule (w_a and w_b). (C) Zoomed out view of chip containing reservoirs at both ends and an entropic trap array. Reprinted from ref. 99 with permission from © AAAS (2000).

entropic trapping. A kinetic model, constructed from equilibrium partitioning theory[104] and a simplified version of Kramers theory,[105] accurately predicts the mobility and trapping time dependence on the DNA length[103] based on an increase in free energy due to reduced configurational freedom and a decrease in free energy due to the reduced electric potential when short molecules cross into the nanoslits. The predictions diverge slightly at DNA lengths above 500 bp when internal conformational changes become important. Satisfyingly, the authors observe a transition between the Ogston and entropic trapping regimes for slits with $R_0/d \approx 1$, where the mobility decreases (increases) with increasing DNA length above (below) the transition. A computational simulation to describe the transport of short DNA molecules through such a nanofilter array has been formulated.[106]

Subsequently, Han and colleagues advanced this design in a two-dimensional periodic nanofilter array capable of the continuous spatial separation of DNA molecules over a broad range of size as well as proteins.[107] The device consists of a series of perpendicular rows of deep channels (300 nm) and shallow channels (55 nm) each 1 μm wide etched in a silicon wafer. An electric field is applied along each direction simultaneously. Molecules are electrophoretically driven along the deep slit until they jump across a nanoslit to the adjacent deep region. Since the probability to escape the deep region is length dependent, the molecules are separated at the bottom of the device into separate streams based on the number of times they

made jumps. The authors used the device in high ionic strength buffer to exhibit a more distinct crossover from Ogston to entropic sieving for by separating DNA with lengths between 50 bp and 23 kbp in minutes. Proteins with negative charge are separated at low ionic strengths due to electrostatic interactions with the negatively charged channel walls once the Debye length is significant compared to the channel height. Molecules with a less negative charge at a given pH are able to make more jumps over the nanoslits per unit time and are deflected farther from the original deep column. Mao and Han recently designed a new version of this device[108] using a fabrication strategy based on anisotropic KOH etching of (110) silicon to generate parallel vertical nanoslits (*e.g.*, the slits are now thin deep slices instead of shallow wide ones). The fabrication requires only standard photolithography, using the growth of a thermal oxide layer on the silicon to narrow the vertical slits to 50 nm widths. The device exhibited similar functionality for DNA and protein separation as the planar version, however, with a volumetric throughput three orders of magnitude larger ($\sim$1 μL h^{-1}).

E.2 Brownian ratchet separation

Independently, Duke and Austin[110] and Ertas[111] realized that since the diffusion of DNA molecules depends on their size (as $L^{-1/2}$, or $L^{-3/5}$ if excluded volume interactions are important), a method that rectifies the Brownian motion could be used as a separation mechanism. Chou *et al.* implemented the scheme[112] by using a sacrificial method technique to create a 350 nm deep nanoslit containing an array of micron sized rectangular obstacles inclined at 45° with respect to an applied electric field (down the channel length). Molecules preferentially follow the field lines between the obstacles, but have a probability to diffuse beyond a boundary in one lateral direction only due to the asymmetric tilting of the obstacles. Since shorter molecules have a larger diffusion constant, they are more likely to be laterally displaced after traveling through the device, allowing separations to be performed continuously. The theory predicts good resolving power in the range $0.02 < D/(\nu a) < 0.3$ where D is the diffusion coefficient, ν is the electrophoretic velocity, and a is the width of the obstacles.[110] The authors compared their results for the measured probability of migration for 15 and 34 kbp DNA to the prediction[110] in the range of DNA velocities between 1 and 15 μm s^{-1} and found reasonable agreement (the device rather unusually outperformed expectations). Cabodi *et al.*[113] improved the design with a new vertical channel injection scheme by using an excimer laser to cut a 10 μm through hole in the silicon wafer that was used to launch a narrow stream of DNA. A mixture of T2 and T7 DNA molecules were separated. Huang *et al.*[114] also improved on the original design using an array of microchannels connected to the separation region as large resistors (relative to the potential drop across the array) to ensure that the field lines did not follow obstacle-hopping trajectories. Huang *et al.* found that DNA molecules below a critical size given by the distance between the obstacles could not be separated with this device, in accordance with a revised theory[115] that takes into account the insulating behavior of the obstacles and finite size of the molecules. The subcritical sized molecules are spread out by the electric field lines, rather than by diffusion, after passing through an obstacle gap and then have equal probability to be deflected in either lateral direction. Huang *et al.*[116] again improved on their design by a factor of 3 in resolution and 10 in speed by tilting the electric field direction at a small angle with respect to the array axis. For the same diffusion constant, tilting the electric field improves the probability of obstacle hopping significantly, increasing the spatial separation distance without broadening the band resolution to the same degree for certain flow velocities. DNA molecules of 48.5 and 164 kbp were separated in 70 min with a resolution of $\sim$4 (separation distance divided by twice the sum of the band widths).

E.3 Electrophoresis in structured media

In one of the first experiments to fabricate an artificial sieving structure to study polymer fractionation in a well characterized topology, Volkmuth and Austin[117] constructed a two-dimensional array of symmetrical obstacles 150 nm high, 1 μm in diameter, with center-to-center spacing of 2 μm, using photolithography on chips of silicon dioxide. They observed that long DNA molecules got hooked around posts and elongated while being electrophoresed through their device. They also observed that mobility depended on length for molecules up to 100 kbp in length, intimating that fabricated structures could serve as a replacement for gel electrophoresis. Turner *et al.*[42] fabricated a conceptually similar structure using a sacrificial technique in combination with e-beam lithography to precisely define the nanoslit height at 100 nm (within 5%), incorporating a symmetric array of square 100 nm obstructions. For some electric field strengths, the mobility of linear 43 kbp DNA was found to be a factor of 2 larger than circular 7 kbp molecules. Kaji *et al.*[118] observed a power-law dependence with negative slope for the mobility *versus* length of DNA between 1 and 25 kbp using electrophoresis through an array of large aspect nanopillars (500 nm diameter, 2700 nm tall with 500 nm spacing). Tabuchi *et al.*[119] rapidly separated DNA from 1 to 15 kbp in length through a core–shell nanosphere suspension with a pressurized loading scheme for narrow band formation just prior to electrophoresis. In an elegant non-lithographic approach, Doyle *et al.*[120] used the self-organized formation of columns of superparamagnetic beads in the presence of an external magnetic field as a sieving obstacle to separate DNA. Mobility was observed to decrease with increasing electric field strength, which was due to DNA deformation, and stretching when contacting the beads. Also, Zeng and Harrison[121] utilized self-assembled colloidal arrays to form three-dimensional nanofluidic sieves in microfluidic devices. By varying the sieving pore sizes formed from different diameter silica particles, the authors electrophoretically separated a range of DNA (0.05 to 50 kbp) and denatured proteins (20 to 200 kDa).

Austin and colleagues continued exploration of their hexagonal obstacle arrays, using pulsed electric fields oriented alternatingly along the axes of the array (separated by 120). They observed under dc conditions that DNA molecules slightly elongate and migrate at a length independent velocity along the channels between the obstacles at fields of 10 V cm^{-1} without hooking.[122] Quite interestingly, upon switching the

field through an obtuse angle, the DNA molecule switches direction with the formerly trailing end now leading the migration. These observations are in agreement with biased reptation models (see ref. 123, for example) that consider the total force on the molecule proportional to the dot product of the molecule's end-to-end vector with the electric field. Consequently, DNA molecules move along the direction bisecting the alternating fields at velocities proportional to $-E\cos(\theta/2)L$, where E is the electric field strength, and θ is the angle between the pulsed fields. They were able to separate DNA molecules of length 169 and 46 kbp with 6% size resolution in 11 min in a 1 cm long chip, using an entropic trap as described in Section E.1 to form a tight plug before launching the DNA. A subsequent version of this device, as depicted in Fig. 9, was improved upon by Huang *et al.*,[109] converting it to a continuous flow separation system with more uniformly distributed electric fields and precise sample injection. By alternating high field strength pulses ($\sim$200 V cm^{-1}) every 50 ms, the authors were able to spatially separate DNA from 100–200 kbp in length with 13% resolution with a throughput of $\sim 10^4$ molecules per second into separate microfluidic output channels as shown in Fig. 10. Austin and colleagues developed another separation technique for DNA in a microfluidic obstacle array based on the asymmetric splitting of laminar flow lines around the obstacles[124] (a factor that determined the critical size for separation in the diffusion based ratchet arrays previously discussed). DNA molecules electrophoresed through the device (in a random coil conformation) follow the field lines unless the radius of gyration is larger than a critical size that depends on the obstacle spacing. Bacterial artificial chromosomes of 61 and 158 kbp were spatially separated in 10 min with resolutions of $\sim$12% and 5% respectively.

E.4 Free solution separation

Cross *et al.*[125] observed electrophoretic separations in 17 nm deep nanoslits (containing neither obstacles nor sieving matrix) for DNA molecules between 2 and 10 kbp using a high ionic strength buffer containing 2% polyvinylpyrrolidone (PVP). The mobility varied approximately as $1/\sqrt{N}$. No separation was found in a 90 nm deep nanoslit for the same length DNA molecules. The authors reported that they were unable to electrophoretically load DNA into the nanochannels without using PVP to suppress the electroosmotic flow. The size-dependent mobility was interpreted within a blob model with a new term introduced to describe surface interactions. Field dependent mobility of lambda DNA was also measured[126] in 20 nm deep nanoslits (containing a similar buffer with 2.5% PVP), where the lambda molecules were observed to become intermittently trapped at various regions in the nanoslits for fields above 300 V cm^{-1}. The authors list steric or dielectrophoretic trapping due to surface roughness as the potential cause. The fused silica wafers in which the slits were fabricated apparently contained 8 nm deep holes as obtained from the (unlisted) manufacturer.

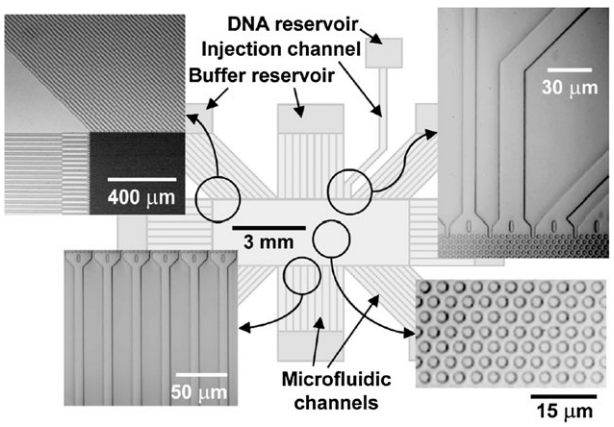

Fig. 9 Structure of a continuous flow DNA sieving matrix integrated with microfluidic channels. A single channel connecting to the DNA reservoir injects DNA through a 28 μm opening. The eight set of microfluidic channels surrounding the sieving matrix connect to buffer reservoirs where external voltages are applied and provide uniform electric fields. Reprinted by permission from Macmillan Publishers Ltd: ref. 109, copyright (2002).

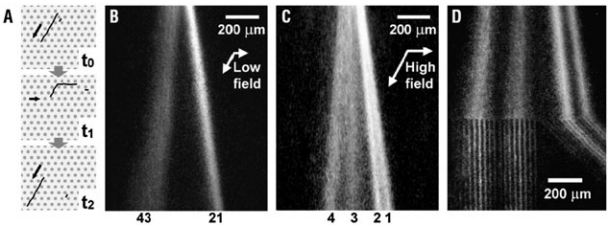

Fig. 10 (A) Schematic illustrating the length based separation principle of the DNA prism. Small and large molecules are initially driven at similar speeds (t_0) until a low field rotated 120° causes reversal of the leading and trailing ends (t_1). When the original field is reapplied (t_2) the ends reverse again with the large molecule in its original track and the small molecule displaced in the average field direction. (B–D) Fluorescence micrographs of continuous DNA separation under different field strengths. (B) Four molecules of length (1) 61 kb; (2) 114 kb; (3) 158 kb; (4) 209 kb are separated into two bands using alternating 32 and 20 V cm^{-1} fields at 2 Hz. (C) All four lengths are separated using 240 and 150 V cm^{-1} fields alternating at 12.5 Hz. (D) Separated molecules are collected in different outlet channels. Reprinted by permission from Macmillan Publishers Ltd: ref. 109, copyright (2002).

Expanding on the earlier work of Petersen *et al.*,[127] Pennathur *et al.*[128] studied the separation of 10–100 bp DNA in nanoslits 40, 100, and 1560 nm in depth under varying salt concentrations leading to a range in the ratio of the Debye length to the channel depth of 0.6–20%. They observed length dependent separation of the DNA that depends both on the Debye length to slit depth and DNA length to slit depth ratio. However, in the 1560 nm deep channel they observed that the separation time increased from largest to smallest DNA length, which is opposite the separation order in the smaller slits (at salt concentrations > 1 mM) and opposite the accepted literature.[129] The difference was attributed to the use of a fluorescein label that alters the charge to mass ratio of the DNA (more significantly as the DNA length decreases). Nevertheless, their data indicate the importance of the electric double layer in shallow nanoslits on DNA mobility. Campbell *et al.*[130] observed that the electrophoretic mobility of lambda DNA in nanochannels increases with decreasing channel diameter. Nanochannels with diameters between $\sim$750 and

165 nm were fabricated in silicon using a focused ion beam. The factor of ~2 difference in mobility seen between the largest and smallest channel was interpreted as a reduced electroosmotic flow in smaller channels due to the low ratio of the channel diameter to Debye length in their experiment.

We also note that the combination of electrophoresis and dielectrophoretic trapping has been employed to separate DNA in microfluidic channels by using insulating obstacle arrays to focus the electric field lines (sometimes termed electrodeless). A mechanism of length dependent DNA polarizability was first proposed by Ajdari and Prost[131] and trapping as a function of frequency, viscosity, and electric field strength was reported by Chou *et al.*[132] for DNA molecules between 0.4 and 40 kbp. Regtmeier *et al.*[133] demonstrated temporal separation for DNA molecules of 48 and 164 kbp using ac fields of ~200 V cm^{-1} and, by measuring trapping lifetimes as a function of the ac field strength, that the polarizability of DNA molecules scales as $N^{0.4\pm0.1}$. Also, size-dependent trajectories of DNA in submicron slits driven with an ac and dc electric field flowing around a sharp corner have been observed.[134] However, the trajectories show little dependence on the applied ac field (and an opposite dependence with length than observed by the previous two papers), leading the authors to speculate on dielectrophoretic forces applied by interactions of DNA with the electric double layer.

F. DNA mapping and sequencing

Mapping a DNA molecule refers to determining the spatial positions along its length where a particular sequence of interest is located. A map provides a so-called barcode of the DNA that may be used to identify a molecule of interest (for example, a pathogen) in a complex sample. The information provided by a map is inferior to obtaining the molecule's complete sequence. However, depending on the specific application's resolution requirement, mapping may provide a distinct advantage in cost and throughput relative to sequencing. Mapping was traditionally performed using restriction enzymes to digest DNA combined with gel electrophoresis for size measurements as in the human genome project.[135] Schwartz and colleagues[136,137] demonstrated a powerful improvement of this technique by optically imaging long (over 100 kbp) individual DNA molecules stretched on glass slides and digested with a restriction enzyme. Stretching and attaching the DNA molecules to the glass surface provides a linear mapping between spatial and genomic position and preserves haplotype information. The technique suffers somewhat from inhomogeneous stretching due to surface interactions. It is clear that flowing linearized and uniformly stretched fluorescent DNA molecules through nanochannels should offer a compelling alternative for mapping. We note that it is cumbersome to quantitatively compare mapping results from different platforms since resolution and throughput are inversely related and it is not always clear the requirements imposed to construct a high-quality map (where the actual experiment time may be much shorter than the computational analysis time).

F.1 Fluorescent mapping in fluidic channels

Riehn *et al.*[138] have integrated optical restriction enzyme digestion analysis with nanofluidic channels to improve the consistency of DNA stretching and throughput. The latter is achieved mostly by capturing the image of a single molecule multiple times after the digestion, with the temporal separation between images being longer than the relaxation time of the molecule to ensure statistical independence. Nanochannels approximately 120 nm on a side produced by FIB were constructed between entry and exit microchannels, the latter containing the enzyme cofactor Mg^{2+}. By application of selected voltages, lambda DNA molecules stained with TOTO-1 and loaded with either of the restriction enzymes SamI and SacI were electrophoretically loaded into the nanochannels while a constant concentration of Mg^{2+} was simultaneously established along the channel. These enzymes each digest the lambda at three locations. Unfortunately, since the digestion required longer than the ~1 s relaxation time of the lambda DNA in these sized channels, the separation between digested fragments was only evident after the fragments had diffused an optically resolvable distance from each other (the fragments did not recoil since they had already equilibrated to their ~40% extended confined length). Also, the spatial location of each digestion was not directly measured but inferred from the relative fluorescent intensity of each fragment and the known length of the DNA molecule, resulting in a systematic ~0.5 kbp bias in the determination of the restriction sites. Still, the authors were able to acquire a tri-fragmented map of lambda DNA at a resolution of 1.5 kbp in approximately one minute.

Instead of restriction enzymes, fluorescent labels hybridized to specific sequences along the DNA can be used to create an optical map. Tegenfeldt *et al.*[139] fabricated a device capable of optical resolution below the diffraction limit by utilizing near field optics. Using e-beam, they created multiple 100 nm wide and 200 nm deep slits in aluminium with perpendicular microfluidic channels (5 μm wide and 1 μm deep) over top. A 100 nm thick layer of SiO_2 protected the aluminium from the channels and ultimately limited the resolution of the device. An array of posts was included at the channel entrance in order to stretch electrophoretically driven DNA molecules. The resolution determined from measurements of fluorescent nanospheres was found to be 200 nm independent of the microscope objective. However, DNA molecules were not uniformly stretched by the post array or sufficiently extended by the large channels, limiting the usefulness of the device for mapping applications. As discussed in D.2, Jo *et al.*[72] used PDMS nanoslits 1 μm wide and 100 nm deep to stretch DNA molecules to 60% of their contour length with a low ionic strength buffer (100-fold dilution of 1× Tris-EDTA). Additionally, they used a nicking enzyme, Nb·BbvCI, that cuts only one strand of double-stranded DNA at a given recognition site. They repaired the nick using fluorochrome-labeled nucleotides (FRET acceptor Alexa Fluor 647) and labeled the DNA backbone with YOYO-1. They were thus able to map three bacterial artificial chromosomes (BAC), using approximately 100 molecules combined, that contained 4 or 5 incorporated labels resulting from the nicking enzyme. Again, by measuring

the relative intensity of each interval between the FRET acceptors and using the known length of the BAC molecules, they were able to map the location of the nicking enzyme sites without bias when compared to the known sequence. The intervals were sized with standard deviations of 2–3 kbp depending on the interval length.

Another interesting approach has been used to optically map DNA molecules in microfluidic channels using hydrodynamic elongational flow in a tapered geometry to achieve stretching as opposed to confinement. The technique is termed direct linear analysis[140,141] (DLA) and relies on labeling intercalated DNA with fluorescent bisPNA tags which are capable of invading double-stranded DNA by displacing one of the strands. DNA molecules are electrophoretically driven at 10–20 μm s^{-1} through two laser interrogation sites along the channel, where both the bisPNA and backbone label are excited at the first spot and the backbone label is excited at the second spot. This two laser spot system allows for the measurement of DNA velocity, which is then used to transform the collected time traces measured by avalanche photodiode detectors into length traces. The authors were able to map a 185 kbp BAC in minutes using 200 molecules with a resolution of 2 kbp by only using molecules stretched to at least 85% of their contour length. This stretching requirement eliminates about 85% of the sample but the high throughput, comparable resolution, and ability to map molecules hundreds of kbp long make this a promising technology. Reccius *et al.*[142] implemented a similar two spot laser setup using nanochannels in preliminary work towards improved mapping resolution. The authors implemented a burst-fitting algorithm that determined that nearly all of the lambda DNA molecules electrophoretically driven through the channel contained a partially folded front (but not back) end. A novel experiment by Wang *et al.*[143] has also used nanochannels to measure repressor protein interactions with individual DNA molecules.

There are additional efforts being made to map or sequence DNA molecules in nanochannels using electronic rather than fluorescent means. Liang and Chou[144] have used NIL and shadow evaporation techniques to fabricate 50 mm long fluidic channels 45 nm in width and depth with a pair of nanowire electrodes transverse to the channel resulting in a metallic gap down to 9 nm in width and 16 nm in height. This allows the measurement of ionic conductance perpendicular to the DNA backbone as the DNA is electrophoresed through the gap. With 1.1 kbp DNA molecules flowing through the channel, reductions in the transverse ionic current of ~350 pA were observed for typical duration times of ~100 mS attributed to blockage of the gap by the insulating DNA molecule. Somewhat large variation in this duration time needs to be further understood and the gap reduced before one can expect sequence specific information to be obtainable.

F.2 Zero-mode waveguides for sequencing

We include work toward DNA sequencing in this and the following subsection as well since sequencing represents the ultimate resolution of mapping. A zero-mode waveguide (ZMW) is a near field nanophotonic structure consisting of a cylindrical hole in a metal cladding film over a transparent substrate.[145] Discussion of ZMWs in this section is somewhat arbitrary since they generally serve to reduce the excitation volume associated with optically excited fluorescence to the order of zeptolitres (10^{-21} l), an improvement of roughly three orders of magnitude compared to confocal microscopy. The reduction in the focal volume results from metal waveguides of a given diameter only supporting propagating modes for wavelengths below a cutoff wavelength equal to 1.7 times the diameter. Longer wavelengths are evanescent and decay exponentially along the waveguide with a characteristic length depending on the wavelength and the wavelength in the medium composing the core. ZMWs are typically fabricated as 40–150 nm diameter holes in a 100 nm thick aluminium film on a fused silica substrate *via* e-beam.[146] The effective observation volume is then limited to approximately the first 10 or 20 nm within the ZMW depending on its diameter. The resulting zeptolitre focal volume of a ZMW allows the observation of single molecule events at micromolar fluorophore concentrations. This concentration is biologically relevant since the enzymatic synthesis of double-stranded DNA by DNA polymerase requires micromolar levels of nucleotides. Consequently, ZMWs have been used for the observation of real time sequencing from single polymerase molecules.[147] By passivating the aluminium film using polyphosphonate chemistry (see Fig. 11), single polymerase molecules are selectively immobilized to the fused silica floor of ZMWs.[148] By detecting four different fluorescently labeled deoxyribonucleoside triphosphate (dNTP) substrates as they are serially incorporated by the polymerase molecule during template selected synthesis real time sequencing is accomplished. By linking the fluorophore to the phosphate group of the dNTP molecule, the fluorophore is naturally cleaved by the polymerase upon nucleotide incorporation, resulting in an unmodified DNA molecule and a fluorescent signal whose duration is given by the catalysis rate plus the much smaller time until the fluorophore diffuses out of the ZMW focal volume. The fabrication and optical requirements of ZMWs allow for massive parallelization so that thousands of sequencing reactions can be observed simultaneously.[149] The polymerase has been shown to synthesize DNA at rates consistent with bulk reactions (several bases per second) and each polymerase molecule can synthesize several kilobases of DNA as shown in Fig. 12.

F.3 Solid-state nanopore sequencing

The literature regarding DNA translocation through nanopores is too large to critically examine in the space remaining. We only review results from solid-state nanopores despite the wealth of information obtained using biological α-haemolysin pores by Kasianowicz and colleagues[150] and refer the reader to interesting reviews and more comprehensive reviews concerning the challenges of nanopore sequencing[151] and recent experimental results.[20] The physical principal behind the original attempts to sequence DNA with nanopores stems from the Coulter counter: the passage of a non-conducting particle or molecule through a small fluidic channel filled with electrolyte increases the Ohmic resistance of the channel leading to a decrease in ionic current or an increase in voltage

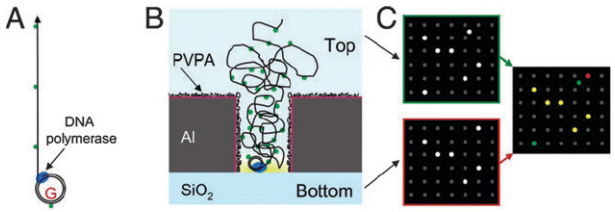

Fig. 11 Principle of sequencing by observing DNA synthesis inside ZMWs. (A) Rolling circle DNA strand displacement synthesis by polymerase produced DNA with fluorescent labels at regular DNA length intervals. (B) Passivated ZMW nanostructures results in selective immobilization of polymerase at the bottom of the ZMW followed by DNA extension reactions. The ZMW observation volume is highlighted in yellow. (C) Fluorescent DNA products imaged from the top and bottom of the arrays. Image analysis confirmed the polymerase immobilization toward the SiO_2 floor (yellow and red dots) instead of on the side and top Al surfaces (green dots) and to demonstrate single molecule occupancy. Reprinted from ref. 148 with permission from © National Academy of Sciences, USA (2008).

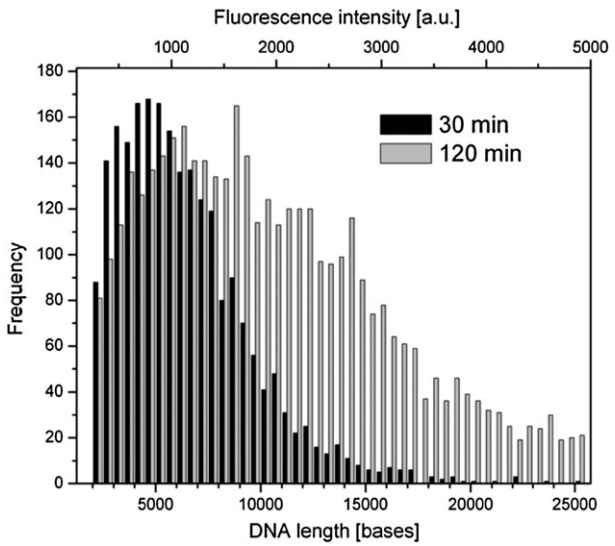

Fig. 12 Length of DNA synthesis in ZMWs. The top x axis displays integrated fluorescent intensities from top-side images after 30 and 120 min of DNA extension using 100 nm average diameter ZMWs. Intensities were converted to DNA size (bottom x axis) by a standard curve using known DNA length samples. Reprinted from ref. 148 with permission from © National Academy of Sciences, USA (2008).

measured across the channel. By passing single-stranded DNA through a nanopore, it was thought that the rectification of the ionic current might also be nucleotide dependent leading to an amplification- and label-free sequencing platform. More recently, it has been proposed that a tunneling current measured transverse to the DNA translocation direction through the nanopore should be sensitive to differences in nucleotide electron orbital configurations providing statistical discrimination for repeated measurements.[152]

As discussed in the Fabrication section, ion beam sculpting[36] and transmission electron microscope[153] techniques have been used to fabricate solid-state nanopores in thin silicon nitride or oxide membranes down to a few nm in diameter. Decreases in ionic currents due to translocation of kbp length double-stranded and single-stranded[154] DNA molecules in a variety of linear and folded configurations have been studied[155] allowing for size based separation based on the measured translocation duration time.[23] Typical reductions in current of $\sim$100 pA are observed for translocation times of $\sim$200 mS for 11 kbp DNA for a potential of 120 mV maintained across the pore.[156] The translocation time has been observed to scale as a power-law with DNA contour length with a measured exponent of 1.27, which has been interpreted based on the hydrodynamic drag of the coil outside the nanopore opposing the electric translocation force.[156] Somewhat surprisingly, it has also been observed that the ionic conductance increases rather than decreases due to DNA translocation[157,158] when the ionic buffer concentration is reduced below 400 mM. The overall effect is attributed to a larger increase in current from the dragging of mobile counterions by the DNA through the pore than from the reduction in current from the geometric blockade below a critical salt concentration. The same observation of increased current for DNA translocation events has been made using 10 mm long inorganic nanotubes 50 nm in diameter.[159] A major criticism of nanopore sequencing has been the inability to control the highly variable translocation times so that picoampere currents can be measured at reasonable detector bandwidths. Keyser *et al.*[160] reported an improvement along these lines by attaching double-stranded DNA molecules to a microsphere held in an optical trap by an infrared laser near a nanopore entrance as shown in Fig. 13. Subsequently, the DNA electrophoreses into the pore and the optical trap can directly measure the force necessary to stall the motion of the DNA molecule. This force is linearly proportional to the applied translocation voltage with a slope of 0.23 pN mV^{-1} independent of the salt concentration from 0.02 to 1 M. The slope has also been shown to be consistent with a $1/\ln(R)$ dependence,[161] where R is the nanopore radius,

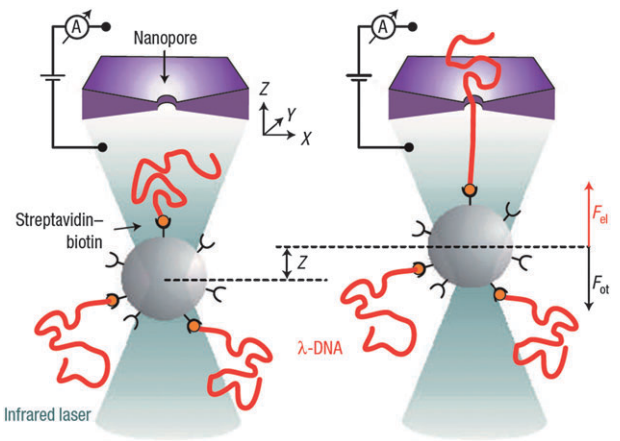

Fig. 13 Schematic illustration of direct force measurements on DNA in a solid-state nanopore. A focused laser beam traps a DNA-coated microsphere near a solid-state nanopore immersed in a saline solution (left). Application of an external voltage drives an ionic current and the DNA molecule into the nanopore. When the DNA enters the nanopore, an electrical force F_{el} is exerted on the bead, which is pulled a distance ΔZ out of the trap until the electrical and optical force F_{ot} are balanced. Reprinted by permission from Macmillan Publishers Ltd: ref. 160, copyright (2006).

for R up to 45 nm. This dependence results from the relatively reduced electroosmotic hydrodynamic drag on the DNA inside the nanopore as the nanopore radius increases.

Conclusions

Nanofluidic systems have been utilized to sensitively probe DNA molecules. Single molecule manipulation experiments have made quantitative measurements of confined polymer conformation and dynamics as well as sub-piconewton entropic forces in nanochannels and nanoslits. These results have been utilized to construct nanofluidic devices for the continuous and rapid sorting of long DNA molecules with a length resolution that compares well to other technologies. Nanofluidic structures are actively being investigated for their unique opportunity to provide optical and electrical high resolution genetic mapping and sequencing information. Many of the reviewed experiments used a model viral DNA molecule less than 1 Mb in length. We anticipate that future investigations will focus on probing genomic length DNA cultivated from more biologically relevant sources, most likely in conjunction with attached proteins and histones. Additionally, nanofluidic systems are likely to be employed for quantitative RNA and gene expression analysis. We envision that nanofluidic systems will become prominent tools within lab on a chip platforms analyzing single biomolecules extracted from single cells.

Notes and references

1 J. Shendure and H. Ji, *Nat. Biotechnol.*, 2008, **26**, 1135–1145.
2 Y. D. Ivanov, V. M. Govorun, V. A. Bykov and A. I. Archakov, *Proteomics*, 2006, **6**, 1399–1414.
3 D. Sproul, N. Gilbert and W. A. Bickmore, *Nat. Rev. Genet.*, 2005, **6**, 775–781.
4 S. Jun and B. Mulder, *Proc. Natl. Acad. Sci. U. S. A.*, 2006, **103**, 12388.
5 P. K. Purohit, J. Kondev and R. Phillips, *Proc. Natl. Acad. Sci. U. S. A.*, 2003, **100**, 3173–3178.
6 S. E. Halford and J. F. Marko, *Nucleic Acids Res.*, 2004, **32**, 3040.
7 M. M. Suzuki and A. Bird, *Nat. Rev. Genet.*, 2008, **9**, 465–476.
8 H. Craighead, *Nature*, 2006, **442**, 387–393.
9 J. T. Mannion, C. H. Reccius, J. D. Cross and H. G. Craighead, *Biophys. J.*, 2006, **90**, 4538–4545.
10 F. Sanger, S. Nicklen and A. R. Coulson, *Proc. Natl. Acad. Sci. U. S. A.*, 1977, **74**, 5463–5467.
11 J. O. Tegenfeldt, C. Prinz, H. Cao, R. L. Huang, R. H. Austin, S. Y. Chou, E. C. Cox and J. C. Sturm, *Anal. Bioanal. Chem.*, 2004, **378**, 1678–1692.
12 C. C. Hsieh and P. S. Doyle, *Korea-Australia Rheology Journal*, 2008, **20**, 127–142.
13 N. Douville, D. Huh and S. Takayama, *Anal. Bioanal. Chem.*, 2008, **391**, 2395–2409.
14 R. B. Schoch, J. Han and P. Renaud, *Rev. Mod. Phys.*, 2008, **80**, 839.
15 P. G. de Gennes, *Scaling Concepts in Polymer Physics*, Cornell University Press, Ithaca, New York, 1979.
16 J. T. Mannion and H. G. Craighead, *Biopolymers*, 2007, **85**, 131–143.
17 G. B. Salieb-Beugelaar, K. D. Dorfman, A. van den Berg and J. C. T. Eijkel, *Lab Chip*, 2009, **9**, 2508–2523.
18 J. C. T. Eijkel and A. V. D. Berg, *Microfluid. Nanofluid.*, 2005, **1**, 249–267.
19 J. Han, J. Fu and R. B. Schoch, *Lab Chip*, 2008, **8**, 23–33.
20 C. Dekker, *Nat. Nanotechnol.*, 2007, **2**, 209–215.
21 J. D. Watson and F. C. Crick, *Nature*, 1953, **171**, 737–738.
22 M. Doi and S. F. Edwards, *The Theory of Polymer Dynamics*, Clarendon, Oxford, UK, 1986.
23 S. Smith, L. Finzi and C. Bustamante, *Science*, 1992, **258**, 1122–1126.
24 P. G. de Gennes, *Macromolecules*, 1976, **9**, 587–593.
25 M. Daoud and P. G. de Gennes, *J. Phys. (Paris)*, 1977, **38**, 85–93.
26 F. Brochard and P. G. de Gennes, *J. Chem. Phys.*, 1977, **67**, 52.
27 F. Brochard, *J. Phys. (Paris)*, 1977, **38**, 1285–1291.
28 T. Odijk, *Macromolecules*, 1983, **16**, 1340–1344.
29 Y. Yang, T. W. Burkhardt and G. Gompper, *Phys. Rev. E: Stat., Nonlinear, Soft Matter Phys.*, 2007, **76**, 011804.
30 W. Reisner, K. J. Morton, R. Riehn, Y. M. Wang, Z. Yu, M. Rosen, J. C. Sturm, S. Y. Chou, E. Frey and R. H. Austin, *Phys. Rev. Lett.*, 2005, **94**, 196101.
31 D. A. Hoagland, E. Arvanitidou and C. Welch, *Macromolecules*, 1999, **32**, 6180–6190.
32 M. Smoluchowski, *Bull. International de l'Academie des Sciences de Cracovie*, 1903, **8**, 182–200.
33 P. Mao and J. Han, *Lab Chip*, 2005, **5**, 837–844.
34 A. Tseng, K. Chen, C. Chen and K. Ma, *IEEE Trans. Electron. Packag. Manuf.*, 2003, **26**, 141–149.
35 K. G. Wang, S. Yue, L. Wang, A. Jin, C. Gu, P. Y. Wang, Y. Feng, Y. Wang and H. Niu, *Microfluid. Nanofluid.*, 2006, **2**, 85–88.
36 J. Li, D. Stein, C. McMullan, D. Branton, M. J. Aziz and J. A. Golovchenko, *Nature*, 2001, **412**, 166–169.
37 S. Y. Chou, P. R. Krauss and P. J. Renstrom, *Appl. Phys. Lett.*, 1995, **67**, 3114.
38 S. Y. Chou, P. R. Krauss, W. Zhang, L. Guo and L. Zhuang, *J. Vac. Sci. Technol., B*, 1997, **15**, 2897–2904.
39 X. Liang, K. J. Morton, R. H. Austin and S. Y. Chou, *Nano Lett.*, 2007, **7**, 3774–3780.
40 H. Cao, Z. Yu, J. Wang, J. O. Tegenfeldt, R. H. Austin, E. Chen, W. Wu and S. Y. Chou, *Appl. Phys. Lett.*, 2002, **81**, 174.
41 Q. Xia, K. J. Morton, R. H. Austin and S. Y. Chou, *Nano Lett.*, 2008, **8**, 3830–3833.
42 S. W. Turner, A. M. Perez, A. Lopez and H. G. Craighead, *J. Vac. Sci. Technol., B*, 1998, **16**, 3835.
43 C. K. Harnett, G. W. Coates and H. G. Craighead, *J. Vac. Sci. Technol., B*, 2001, **19**, 2842.
44 H. A. Reed, C. E. White, V. Rao, S. A. Allen, C. L. Henderson and P. A. Kohl, *J. Micromech. Microeng.*, 2001, **11**, 733–738.
45 D. Bhusari, H. Reed, M. Wedlake, A. Padovani, S. Allen and P. Kohl, *J. Microelectromech. Syst.*, 2001, **10**, 400–408.
46 D. A. Czaplewski, J. Kameoka, R. Mathers, G. W. Coates and H. G. Craighead, *Appl. Phys. Lett.*, 2003, **83**, 4836–4838.
47 C. W. Kuo, K. H. Wei, C. H. Lin, J. Y. Shiu and P. Chen, *Electrophoresis*, 2008, **29**, 2931–2938.
48 D. Huh, K. L. Mills, X. Zhu, M. A. Burns, M. D. Thouless and S. Takayama, *Nat. Mater.*, 2007, **6**, 424–428.
49 R. Riehn and R. H. Austin, *Anal. Chem.*, 2006, **78**, 5933–5934.
50 T. Perkins, D. Smith, R. Larson and S. Chu, *Science*, 1995, **268**, 83–87.
51 A. Sischka, K. Toensing, R. Eckel, S. D. Wilking, N. Sewald, R. Ros and D. Anselmetti, *Biophys. J.*, 2005, **88**, 404–411.
52 O. B. Bakajin, T. A. J. Duke, C. F. Chou, S. S. Chan, R. H. Austin and E. C. Cox, *Phys. Rev. Lett.*, 1998, **80**, 2737–2740.
53 D. Long, J. L. Viovy and A. Ajdari, *Phys. Rev. Lett.*, 1996, **76**, 3858–3861.
54 L. J. Guo, X. Cheng and C. F. Chou, *Nano Lett.*, 2004, **4**, 69–73.
55 J. O. Tegenfeldt, C. Prinz, H. Cao, S. Chou, W. W. Reisner, R. Riehn, Y. M. Wang, E. C. Cox, J. C. Sturm and P. Silberzan, *Proc. Natl. Acad. Sci. U. S. A.*, 2004, **101**, 10979–10983.
56 A. Balducci, P. Mao, J. Y. Han and P. S. Doyle, *Macromolecules*, 2006, **39**, 6273–6281.
57 F. Persson, P. Utko, W. Reisner, N. B. Larsen and A. Kristensen, *Nano Lett.*, 2009, **9**, 1382–1385.
58 C. H. Reccius, J. T. Mannion, J. D. Cross and H. G. Craighead, *Phys. Rev. Lett.*, 2005, **95**, 268101–268101.
59 S. Jun, D. Thirumalai and B. Y. Ha, *Phys. Rev. Lett.*, 2008, **101**, 138101.
60 C. C. Hsieh, A. Balducci and P. S. Doyle, *Macromolecules*, 2007, **40**, 5196–5205.

61 R. M. Jendrejack, D. C. Schwartz, M. D. Graham and J. J. de Pablo, *J. Chem. Phys.*, 2003, **119**, 1165–1173.
62 J. L. Harden and M. Doi, *J. Phys. Chem.*, 1992, **96**, 4046–4052.
63 A. Balducci, C. Hsieh and P. S. Doyle, *Phys. Rev. Lett.*, 2007, **99**, 238102–238104.
64 D. Stein, F. H. J. van der Heyden, W. J. A. Koopmans and C. Dekker, *Proc. Natl. Acad. Sci. U. S. A.*, 2006, **103**, 15853.
65 P. K. Lin, C. C. Fu, Y. L. Chen, Y. R. Chen, P. K. Wei, C. H. Kuan and W. S. Fann, *Phys. Rev. E: Stat., Nonlinear, Soft Matter Phys.*, 2007, **76**, 011806.
66 E. A. Strychalski, S. L. Levy and H. G. Craighead, *Macromolecules*, 2008, **41**, 7716–7721.
67 D. J. Bonthuis, C. Meyer, D. Stein and C. Dekker, *Phys. Rev. Lett.*, 2008, **101**, 108303–108304.
68 P. S. Doyle, private communication.
69 P. K. Lin, K. Lin, C. C. Fu, K. C. Lee, P. K. Wei, W. W. Pai, P. H. Tsao, Y. L. Chen and W. S. Fann, *Macromolecules*, 2009, **42**, 1770–1774.
70 T. Odijk, *J. Polym. Sci.*, 1977, **15**, 477–483.
71 J. Skolnick and M. Fixman, *Macromolecules*, 1977, **10**, 944–948.
72 K. Jo, D. M. Dhingra, T. Odijk, J. J. de Pablo, M. D. Graham, R. Runnheim, D. Forrest and D. C. Schwartz, *Proc. Natl. Acad. Sci. U. S. A.*, 2007, **104**, 2673.
73 W. Reisner, J. P. Beech, N. B. Larsen, H. Flyvbjerg, A. Kristensen and J. O. Tegenfeldt, *Phys.Rev. Lett.*, 2007, **99**, 58302.
74 D. Stigter, *Biopolymers*, 1977, **16**, 1435–1448.
75 D. Stigter, *J. Colloid Interface Sci.*, 1975, **53**, 72.
76 C. C. Hsieh, A. Balducci and P. S. Doyle, *Nano Lett.*, 2008, **8**, 1683–1688.
77 C. Zhang, F. Zhang, J. A. van Kan and J. R. C. Van der Maarel, *J. Chem. Phys.*, 2008, **128**, 225109.
78 H. Benoit and P. Doty, *J. Phys. Chem.*, 1953, **57**, 958–963.
79 T. Odijk, *Phys. Rev. E: Stat., Nonlinear, Soft Matter Phys.*, 2008, **77**, 060901.
80 E. Arvanitidou and D. Hoagland, *Phys. Rev. Lett.*, 1991, **67**, 1464–1466.
81 D. L. Smisek and D. A. Hoagland, *Science*, 1990, **248**, 1221–1223.
82 D. A. Hoagland and M. Muthukumar, *Macromolecules*, 1992, **25**, 6696–6698.
83 G. W. Slater and S. Y. Wu, *Phys. Rev. Lett.*, 1995, **75**, 164–167.
84 J. Han and H. G. Craighead, *J. Vac. Sci. Technol., A*, 1999, **17**, 2142.
85 S. W. P. Turner, M. Cabodi and H. G. Craighead, *Phys. Rev. Lett.*, 2002, **88**, 128103–128103.
86 S. Manneville, P. Cluzel, J. L. Viovy, D. Chatenay and F. Caron, *Europhys. Lett.*, 1996, **36**, 413–418.
87 T. T. Perkins, S. R. Quake, D. E. Smith and S. Chu, *Science*, 1994, **264**, 822–826.
88 S. L. Levy, J. T. Mannion, J. Cheng, C. H. Reccius and H. G. Craighead, *Nano Lett.*, 2008, **8**, 3839–3844.
89 A. Arnold and S. Jun, *Phys. Rev. E: Stat., Nonlinear, Soft Matter Phys.*, 2007, **76**, 031901.
90 W. Reisner, N. B. Larsen, H. Flyvbjerg, J. O. Tegenfeldt and A. Kristensen, *Proc. Natl. Acad. Sci. U. S. A.*, 2009, **106**, 79–84.
91 M. Krishnan, Z. Petrasek, I. Monch and P. Schwille, *Small*, 2008, **4**, 1900–1906.
92 M. Krishnan, I. Monch and P. Schwille, *Nano Lett.*, 2007, **7**, 1270–1275.
93 R. Riehn, R. H. Austin and J. C. Sturm, *Nano Lett.*, 2006, **6**, 1973–1976.
94 N. C. Stellwagen and C. Gelfi, *Biopolymers*, 1997, **42**, 687–703.
95 H. Chou, C. Spence, A. Scherer and S. Quake, *Proc. Natl. Acad. Sci. U. S. A.*, 1999, **96**, 11–13.
96 M. Foquet, J. Korlach, W. Zipfel, W. W. Webb and H. G. Craighead, *Anal. Chem.*, 2002, **74**, 1415–1422.
97 J. Han, S. W. Turner and H. G. Craighead, *Phys. Rev. Lett.*, 1999, **83**, 1688–1691.
98 J. Han and H. G. Craighead, *Anal. Chem.*, 2002, **74**, 394–401.
99 J. Han and H. G. Craighead, *Science*, 2000, **288**, 1026–1029.
100 F. Tessier, J. Labrie and G. W. Slater, *Macromolecules*, 2002, **35**, 4791–4800.
101 M. Cabodi, S. W. P. Turner and H. G. Craighead, *Anal. Chem.*, 2002, **74**, 5169–5174.
102 J. Fu, P. Mao and J. Han, *Appl. Phys. Lett.*, 2005, **87**, 263902.
103 J. Fu, J. Yoo and J. Han, *Phys. Rev. Lett.*, 2006, **97**, 018103–018104.
104 J. C. Giddings, E. Kucera, C. P. Russell and M. N. Myers, *J. Phys. Chem.*, 1968, **72**, 4397–4408.
105 A. Ajdari and J. Prost, *Proc. Natl. Acad. Sci. U. S. A.*, 1991, **88**, 4468–4471.
106 H. Bow, Y. Cheng and J. Han, *Electrophoresis*, 2008, **29**, 329–339.
107 J. Fu, R. B. Schoch, A. L. Stevens, S. R. Tannenbaum and J. Han, *Nat. Nanotechnol.*, 2007, **2**, 121–128.
108 P. Mao and J. Han, *Lab Chip*, 2009, **9**, 586–591.
109 L. R. Huang, J. O. Tegenfeldt, J. J. Kraeft, J. C. Sturm, R. H. Austin and E. C. Cox, *Nat. Biotechnol.*, 2002, **20**, 1048–1051.
110 T. A. J. Duke and R. H. Austin, *Phys. Rev. Lett.*, 1998, **80**, 1552.
111 D. Ertas, *Phys. Rev. Lett.*, 1998, **80**, 1548–1551.
112 C. Chou, O. Bakajin, S. W. P. Turner, T. A. J. Duke, S. S. Chan, E. C. Cox, H. G. Craighead and R. H. Austin, *Proc. Natl. Acad. Sci. U. S. A.*, 1999, **96**, 13762–13765.
113 M. Cabodi, Y. F. Chen, S. W. P. Turner, H. G. Craighead and R. H. Austin, *Electrophoresis*, 2002, **23**, 3496–3503.
114 L. R. Huang, P. Silberzan, J. O. Tegenfeldt, E. C. Cox, J. C. Sturm, R. H. Austin and H. Craighead, *Phys. Rev. Lett.*, 2002, **89**, 178301.
115 R. H. Austin, N. Darnton, R. Huang, J. Sturm, O. Bakajin and T. Duke, *Appl. Phys. A: Mater. Sci. Process.*, 2002, **75**, 279–284.
116 L. R. Huang, E. C. Cox, R. H. Austin and J. C. Sturm, *Anal. Chem.*, 2003, **75**, 6963–6967.
117 W. D. Volkmuth and R. H. Austin, *Nature*, 1992, **358**, 600–602.
118 N. Kaji, Y. Tezuka, Y. Takamura, M. Ueda, T. Nishimoto, H. Nakanishi, Y. Horiike and Y. Baba, *Anal. Chem.*, 2004, **76**, 15–22.
119 M. Tabuchi, M. Ueda, N. Kaji, Y. Yamasaki, Y. Nagasaki, K. Yoshikawa, K. Kataoka and Y. Baba, *Nat. Biotechnol.*, 2004, **22**, 337–340.
120 P. S. Doyle, J. Bibette, A. Bancaud and J. Viovy, *Science*, 2002, **295**, 2237.
121 Y. Zeng and D. J. Harrison, *Anal. Chem.*, 2007, **79**, 2289–2295.
122 T. A. J. Duke, R. H. Austin, E. C. Cox and S. S. Chan, *Electrophoresis*, 1996, **17**, 1075–1079.
123 J. L. Viovy, *Rev. Mod. Phys.*, 2000, **72**, 813–872.
124 L. R. Huang, E. C. Cox, R. H. Austin and J. C. Sturm, *Science*, 2004, **304**, 987–990.
125 J. D. Cross, E. A. Strychalski and H. G. Craighead, *J. Appl. Phys.*, 2007, **102**, 024701.
126 G. B. Salieb-Beugelaar, J. Teapal, J. V. Nieuwkasteele, D. Wijnperle, J. O. Tegenfeldt, F. Lisdat, A. van den Berg and J. C. T. Eijkel, *Nano Lett.*, 2008, **8**, 1785–1790.
127 N. J. Petersen, J. P. Alarie, S. A. Jacobson and J. M. Ramsey, *Proc. 7th Int. Conf. Miniaturized Chem. Biochem. Anal. Syst.*, Squaw Valley, California, 2003.
128 S. Pennathur, F. Baldessari, J. G. Santiago, M. G. Kattah, J. B. Steinman and P. J. Utz, *Anal. Chem.*, 2007, **79**, 8316–8322.
129 P. G. Righetti, C. Gelfi and M. R. D'Acunto, *Electrophoresis*, 2002, **23**, 1361–1374.
130 L. C. Campbell, M. J. Wilkinson, A. Manz, P. Camilleri and C. J. Humphreys, *Lab Chip*, 2004, **4**, 225–229.
131 A. Ajdari and J. Prost, *Proc. Natl. Acad. Sci. U. S. A.*, 1991, **88**, 4468–4471.
132 C. F. Chou, J. O. Tegenfeldt, O. Bakajin, S. S. Chan, E. C. Cox, N. Darnton, T. Duke and R. H. Austin, *Biophys. J.*, 2002, **83**, 2170–2179.
133 J. Regtmeier, T. T. Duong, R. Eichhorn, D. Anselmetti and A. Ros, *Anal. Chem.*, 2007, **79**, 3925–3932.
134 G. O. F. Parikesit, A. P. Markesteijn, O. M. Piciu, A. Bossche, J. Westerweel, I. T. Young and Y. Garini, *Biomicrofluidics*, 2008, **2**, 024103–024114.
135 The International Human Genome Mapping Consortium, *Nature*, 2001, **409**, 934–941.
136 E. V. Armbrust, J. A. Berges, C. Bowler, B. R. Green, D. Martinez, N. H. Putnam, S. Zhou, A. E. Allen, K. E. Apt, M. Bechner, M. A. Brzezinski, B. K. Chaal, A. Chiovitti, A. K. Davis, M. S. Demarest, J. C. Detter, T. Glavina, D. Goodstein, M. Z. Hadi, U. Hellsten, M. Hildebrand, B. D. Jenkins, J. Jurka, V. V. Kapitonov, N. Kroger, W. W. Y. Lau, T. W. Lane, F. W. Larimer, J. C. Lippmeier, S. Lucas,

M. Medina, A. Montsant, M. Obornik, M. S. Parker, B. Palenik, G. J. Pazour, P. M. Richardson, T. A. Rynearson, M. A. Saito, D. C. Schwartz, K. Thamatrakoln, K. Valentin, A. Vardi, F. P. Wilkerson and D. S. Rokhsar, *Science*, 2004, **306**, 79–86.
137 E. T. Dimalanta, A. Lim, R. Runnheim, C. Lamers, C. Churas, D. K. Forrest, J. J. de Pablo, M. D. Graham, S. N. Coppersmith, S. Goldstein and D. C. Schwartz, *Anal. Chem.*, 2004, **76**, 5293–5301.
138 R. Riehn, M. Lu, Y. M. Wang, S. F. Lim, E. C. Cox and R. H. Austin, *Proc. Natl. Acad. Sci. U. S. A.*, 2005, **102**, 10012–10016.
139 J. O. Tegenfeldt, O. Bakajin, C. F. Chou, S. S. Chan, R. Austin, W. Fann, L. Liou, E. Chan, T. Duke and E. C. Cox, *Phys. Rev. Lett.*, 2001, **86**, 1378.
140 E. Y. Chan, N. M. Goncalves, R. A. Haeusler, A. J. Hatch, J. W. Larson, A. M. Maletta, G. R. Yantz, E. D. Carstea, M. Fuchs, G. G. Wong, S. R. Gullans and R. Gilmanshin, *Genome Res.*, 2004, **14**, 1137.
141 K. M. Phillips, J. W. Larson, G. R. Yantz, C. M. D'Antoni, M. V. Gallo, K. A. Gillis, N. M. Goncalves, L. A. Neely, S. R. Gullans and R. Gilmanshin, *Nucleic Acids Res.*, 2005, **33**, 5829.
142 C. H. Reccius, S. M. Stavis, J. T. Mannion, L. P. Walker and H. G. Craighead, *Biophys. J.*, 2008, **95**, 273–286.
143 Y. M. Wang, J. O. Tegenfeldt, W. Reisner, R. Riehn, X. J. Guan, L. Guo, I. Golding, E. C. Cox, J. Sturm and R. H. Austin, *Proc. Natl. Acad. Sci. U. S. A.*, 2005, **102**, 9796–9801.
144 X. Liang and S. Y. Chou, *Nano Lett.*, 2008, **8**, 1472–1476.
145 M. J. Levene, J. Korlach, S. W. Turner, M. Foquet, H. G. Craighead and W. W. Webb, *Science*, 2003, **299**, 682–686.
146 M. Foquet, K. T. Samiee, X. Kong, B. P. Chauduri, P. M. Lundquist, S. W. Turner, J. Freudenthal and D. B. Roitman, *J. Appl. Phys.*, 2008, **103**, 034301–034309.
147 J. Eid, A. Fehr, J. Gray, K. Luong, J. Lyle, G. Otto, P. Peluso, D. Rank, P. Baybayan, B. Bettman, A. Bibillo, K. Bjornson, B. Chaudhuri, F. Christians, R. Cicero, S. Clark, R. Dalal, A. deWinter, J. Dixon, M. Foquet, A. Gaertner, P. Hardenbol, C. Heiner, K. Hester, D. Holden, G. Kearns, X. Kong, R. Kuse, Y. Lacroix, S. Lin, P. Lundquist, C. Ma, P. Marks, M. Maxham, D. Murphy, I. Park, T. Pham, M. Phillips, J. Roy, R. Sebra, G. Shen, J. Sorenson, A. Tomaney, K. Travers, M. Trulson, J. Vieceli, J. Wegener, D. Wu, A. Yang, D. Zaccarin, P. Zhao, F. Zhong, J. Korlach and S. Turner, *Science*, 2009, **323**, 133–138.
148 J. Korlach, P. J. Marks, R. L. Cicero, J. J. Gray, D. L. Murphy, D. B. Roitman, T. T. Pham, G. A. Otto, M. Foquet and S. W. Turner, *Proc. Natl. Acad. Sci. U. S. A.*, 2008, **105**, 1176.
149 P. M. Lundquist, C. F. Zhong, P. Zhao, A. B. Tomaney, P. S. Peluso, J. Dixon, B. Bettman, Y. Lacroix, D. P. Kwo, E. McCullough, M. Maxham, K. Hester, P. McNitt, D. M. Grey, C. Henriquez, M. Foquet, S. W. Turner and D. Zaccarin, *Opt. Lett.*, 2008, **33**, 1026–1028.
150 J. J. Kasianowicz, E. Brandin, D. Branton and D. Deamer, *Proc. Natl. Acad. Sci. U. S. A.*, 1996, **93**, 13770–13773.
151 D. Branton, D. W. Deamer, A. Marziali, H. Bayley, S. A. Benner, T. Butler, M. Di Ventra, S. Garaj, A. Hibbs, X. Huang, S. B. Jovanovich, P. S. Krstic, S. Lindsay, X. S. Ling, C. H. Mastrangelo, A. Meller, J. S. Oliver, Y. V. Pershin, J. M. Ramsey, R. Riehn, G. V. Soni, V. Tabard-Cossa, M. Wanunu, M. Wiggin and J. A. Schloss, *Nat. Biotechnol.*, 2008, **26**, 1146–1153.
152 J. Lagerqvist, M. Zwolak and M. Di Ventra, *Nano Lett.*, 2006, **6**, 779–782.
153 A. J. Storm, J. H. Chen, X. S. Ling, H. W. Zandbergen and C. Dekker, *Nat. Mater.*, 2003, **2**, 537–540.
154 D. Fologea, M. Gershow, B. Ledden, D. S. McNabb, J. A. Golovchenko and J. Li, *Nano Lett.*, 2005, **5**, 1905–1909.
155 J. Li, M. Gershow, D. Stein, E. Brandin and J. A. Golovchenko, *Nat. Mater.*, 2003, **2**, 611–615.
156 A. J. Storm, C. Storm, J. Chen, H. Zandbergen, J. Joanny and C. Dekker, *Nano Lett.*, 2005, **5**, 1193–1197.
157 H. Chang, F. Kosari, G. Andreadakis, M. A. Alam, G. Vasmatzis and R. Bashir, *Nano Lett.*, 2004, **4**, 1551–1556.
158 R. M. M. Smeets, U. F. Keyser, D. Krapf, M. Y. Wu, N. H. Dekker and C. Dekker, *Nano Lett.*, 2006, **6**, 89–95.
159 R. Fan, R. Karnik, M. Yue, D. Li, A. Majumdar and P. Yang, *Nano Lett.*, 2005, **5**, 1633–1637.
160 U. F. Keyser, B. N. Koeleman, S. van Dorp, D. Krapf, R. M. M. Smeets, S. G. Lemay, N. H. Dekker and C. Dekker, *Nat. Phys.*, 2006, **2**, 473–477.
161 S. van Dorp, U. F. Keyser, N. H. Dekker, C. Dekker and S. G. Lemay, *Nat. Phys.*, 2009, **5**, 347–351.

